Biomedical Materials & Devices (2023) 1:805–824
https://doi.org/10.1007/s44174-022-00055-8

ORIGINAL ARTICLE

Long-Term In Vivo Response of a Polyurethane Gastric Implant for Treating Gastro-Oesophageal Reflux Diseases: A Comparison of Different Surface Treatments

Håvard J. Haugen[1] · Armin Schneider[2,3] · Henning Schlicht[4] · Hongbin Wu[4] · Emmanouil Doundoulakis[2] · Dirk Wilhelm[2] · Markus Eblenkamp[4] · Erich Wintermantel[4] · Hubertus Feussner[2,5]

Received: 1 November 2022 / Accepted: 22 November 2022 / Published online: 2 December 2022

Abstract

Gastro oesophagael reflux disease (GORD) is common in the Western hemisphere. Patients with regurgitated reflux are typically treated with fundoplication surgery. We present a newly designed polyurethane implant which passively aids the sphincter in reducing gastric fluids within the oesophagus. The gastric implant has an open porous inner side which allows for tissue ingrowth from the oesophagus and thus allows for fixation around the sphincter. In addition, a device for minimally invasive surgery of this implant was developed and used in a pig model. The unmodified GORD implant was placed around the pig's oesophagus with unsatisfactory results, leading to insufficient fixation at the implantation site and scarring tissue leading to dysphagia. In addition, two surface modifications, plasma activation and TiO_2 deposition were used to improve the implant's host tissue response. The biocompatibility effects of the surface treatments and sterilisation method on the implant were investigated in vitro and in vivo. In vitro tests found that the plasma activation and TiO2 deposition have effectively enhanced the surface hydrophilicity and, consequently, the cell response to the implant. In addition, the gamma sterilisation harmed the plasma-activated implant. The plasma activation was more effective than TiO_2 deposition as a surface treatment method for improving the tissue response of this implant in vivo. In addition, the in vivo experiment proved tissue ingrowth as deep as 1 mm into the porous structure of the implant. The GORD implants were encapsulated wholly in fibrous tissue; however, the capsule thickness diminished over time. Finally, the TiO_2-coated implants showed the poorest histocompatibility, contradictory to the in vitro findings. This study shows that it is possible to produce a plasma-treated porous polyurethane gastric implant that allows for fibrous tissue ingrowth, reduced in vivo encapsulation, and enhanced chemical properties.

✉ Håvard J. Haugen
h.j.haugen@odont.uio.no

[1] Department of Biomaterials, Institute for Clinical Dentistry, University of Oslo, Blindern, PO Box 1109, NO-0317 Oslo, Norway

[2] Minimally Invasive Therapy and Intervention Research Group MITI, Klinikum rechts der Isar, Technische Universität München, Trogerstraße 26, 81675 Munich, Germany

[3] Jade University of Applied Sciences, Friedrich-Paffrath-Straße 101, 26389 Wilhelmshaven, Germany

[4] Department and Chair for Medical Engineering, Technische Universität München, Boltzmannstraße 15, 85748 Garching, Germany

[5] Department of Surgery, Klinikum rechts der Isar, Technische Universität München, Ismaningerstraße 22, 81675 Munich, Germany

Graphical Abstract

Model of the implant with an inner porous and an outer non-porous surface. The hypothesis was that the porous surface allows for fibroblastic infiltration into the porous structure (A) and fixation by scarring at the point of implantation, the lower oesophageal sphincter (LOS). The outer side is smooth (B), which hinders neighbouring tissue attachments. In addition, a Nitinol ring (C) aids the implant in exerting pressure around the LOS, thus reducing sphincter volume. In addition, this metal ring aids visualisation with, e.g. X-ray or CT during post-therapy follow-ups. The open, flexible design eases the freeing of the ring in a stretched position and placement around the cardia (D-F). The internal diameter of 28 mm prevents stenosis but markedly reinforces the lower oesophagal sphincter. In addition, its size allows for minimally invasive surgery.

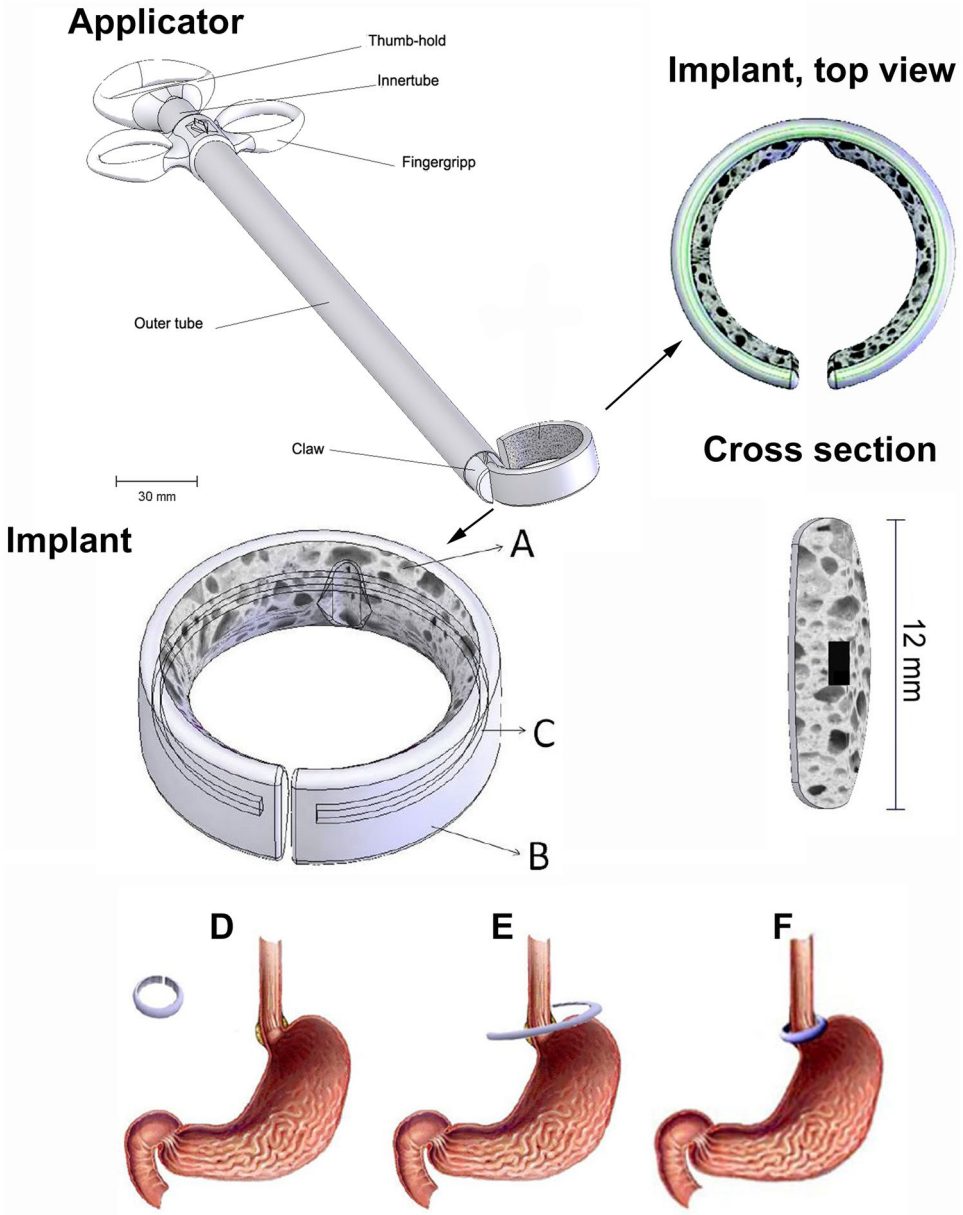

Keywords Polyurethane · Medical device · Supercritical fluid (SCF) · Porous implant · Long-term in vivo response · Surface treatment · Gastroenterology · Gastro oesophagael reflux diseases · Transluminal endoscopic surgery

Introduction

Gastric oesophagael reflux disease (GORD) is common in the western hemisphere [1–4], and as many as one out of ten experience gastric refluxes weekly[3]. Anti-reflux medicine is one of the most prescribed primary-care medications. In worst-case scenarios, the long-term effects of heartburn will develop into cancer, which causes a reduction in life quality [5]. Therefore, heartburn symptoms should be taken earnestly, and suitable treatment options.

There are published guidelines on disease management [6–9]. The consensus is that "PPIs are the most effective therapy and should be used as the first therapy to control GORD after the clinical diagnosis has been made" [10]. Medications such as proton pump inhibitors (PPI) are costly; unfortunately, these medications must be administered lifelong [11]. Surgical intervention is the usual treatment if symptoms persist, even with PPI [12]. Longstanding treatment aims to administer the lowest medication level possible [13]. Laparoscopic fundoplication surgery, the gold standard surgery procedure, obliges a skilled surgeon and should only be used for particular cases [4], e.g. for PPI intolerance or resistance to long-term medication usage amongst patients [12]. Surgery is not 100% satisfying for most patients [14, 15] due to the technical demanding laparoscopic fundoplication, where surgeons' skills and experience govern its success [16]. An additional disadvantage is the fundoplication unsuccessfulness occurring in up to 40% of such cases [17, 18]. Other complications, such as dysphagia, inability to belch, and bloating symptoms, are reported in up to twenty percent of fundoplication surgery[19–21]. Thus there is a demand for a safer, more efficient and less invasive therapy than fundoplication surgery.

In the 70 s, Jean-Pierre Angelchik developed an implant for reflux disease treatment called the Angelchik Anti-reflux Prothesis (APP) [22]. The immediate post-operative results were superior to the standard surgical method Fundoplikatio, and 30,000 implants were inserted [23]. Only in long-term studies did the implant's weaknesses become apparent, namely primarily the triggering of dysphagia and lack of fixation as the Lower Oesophageal Sphincter (LOS) [24, 25]. Further studies presented many complications and a less effective pH reduction than fundoplication [26, 27], which led to the withdrawal of the APP implant from the market. We introduce an alternative to laparoscopic fundoplication inspired by the APP, where a circle-shaped polyurethane implant is placed around the oesophagus's sphincter. Since this implant exerts a passive pressure upon the LOS and thus supports the sphincter, the gastric reflux into the oesophagus is reduced (Graphical abstract (GA), D-F). The pressure aid to the sphincter is a key advantage of the gastric implant since LOS function loss is the main cause of the GORD. Two forces are applied to LOS, one by the implant itself and another by a superelastic metal, nitinol (Graphical abstract (GA), B). This porous inner side (GA, A) is the hypothesis to allow for tissue ingrowth and prevent migration along the oesophagus or perforation of the gastric implant. This feature prevents unfortunate dislocation, as seen by the APP implant, which has a smooth silicon surface towards the oesophagus. Another advantage over the APP is a 20-times weight reduction, which asserts less gravitational forces to the implant. Clinical trials of APP failed due to its migration, perforation or dysphagia due to uncontrolled encapsulation [23, 26, 28]. The outside of the implant is kept smooth to prevent the growth of nearby lying tissues (GA. B) and reduce encapsulation. It has an internal diameter of 28 mm and a nominal wall thickness of 3 mm, allowing natural orifice transluminal endoscopic surgery (NOTES). GORD is a common disease [29]. The yearly need for GORD implants in Europe alone is estimated at 250,000. Therefore, large-scale implant production is essential. Our GORD implant is produced by injection moulding with a specialised design mould [30], where supercritical fluid (SCF) was injected into the polymer during production to enable an open porous structure. Medical grade thermoplastic polyurethane (TPU, Texin® 985, Bayer, Pa, USA) was selected as raw material owing to its outstanding elastic properties, biocompatible and bioinertness [31–34]. Although it has been shown that it is possible to produce a highly porous GORD implant with the SCF with porosity up to 75% and acceptable in vitro response [30, 35, 36], the gastric implant has not been tested in vivo condition. SCF is a popular method to provide open porous in medical polymers [37–41]. The main hypothesis of the porous inner structure was to prevent the implant from sliding along the oesophagus (see GA, D), however so far, we have not shown that the porous structure inside the polyurethane indeed fixates the gastric implant at the Lower Oesophageal Sphincter (LOS). Therefore, the current study aimed to evaluate the gastric implant's in vivo performance and determine whether any surface modification was necessary to induce tissue ingrowth into the porous structure. Both a pig and rabbit were used as animal models. The successful functionality and performance in minimally invasive surgery natural orifice transluminal endoscopic surgery with this gastric implant is published elsewhere and will not be repeated here [42]. Established TPU surface modification techniques was used to allow for fast-forward regulatory processes and clinical translation.

Material and Methods

Implant Production

The raw material was medical-grade thermoplastic polyurethane TPU (Texin® 985, Bayer, Pa, USA). An injection moulding machine (KM 125-520C2, Krauss Maffei Technologies GmbH, Munich, Germany) with a supercritical fluid CO_2 (Trexel Inc., Woburn, MA, USA) was used for the production of the porous/non-porous GORD implant. The injection mould was custom-made. The production details and parameters have been investigated and described elsewhere and are therefore not further elaborated [30, 36].

First Animal Trial (Pig Study)

The Munich miniature pig Troll was selected as the animal model because it has an appropriate growth rate and no longer has gains weighted significantly after the GORD implant implantation at about three months. It grows to around 55–60 cm and can reach a final weight of 60–70 kg. The animal experiment series includes eight animals. One day before the operation, the experimental animal was taken from an external board to the animal care of Klinikum Rechts Der Isar, Technische Universität Munich. Access to the cages was limited to persons; trained laboratory animal keepers monitored the animal. A light–dark light program with twilight phases simulates daylight conditions. Special feed and tap water from an automatic nipple drinker are available indefinitely. The animal was fasted for 10 h prior to surgery. 3.6.2 Anaesthesia and surgery. General anaesthesia was initiated with a drug mixture (2 mg/kg azaperone, 10–15 mg/kg ketamine, 0.5–1.0 mg/animal atropine), injected intramuscularly into the experimental animal in the animal housing room. The sedated animal was given access to the marginal vein in the ear, through which propofol was introduced until it could be intubated. After intubation, the experimental animal was artificially ventilated. To maintain anaesthesia, propofol was given as a continuous drip infusion (approx. 7 mg/kg/h) and fentanyl as required (approx. 1.5 ml/bolus). During the surgical procedure, the animal was monitored via capnometry, pulse oximetry, blood pressure measurement, ECG and temperature probe, and the depth of anaesthesia and ventilation were readjusted if necessary. In order to compensate for the fluid loss, fluid was permanently administered intravenously at the maintenance requirement level (10–20 ml/kg/h). The abdominal cavity was opened, the oesophagocardial transition was shown, and its musculature was completely removed over a width of approx. 2 cm, which induced reflux disease in the experimental animal. Strict care was taken to ensure that neither the two vagus cords nor the mucosa of the oesophagus were injured, as this would falsify the results. In human patients, the reflux disease would already be acute, and the muscles would not be removed. Finally, the GORD implant was inserted, and the peritoneum, fascia and skin were closed with sutures. After waking up from the anaesthetic, the test animal received water and liquid food (Fresubin), and from the third post-operative day, it was switched back to normal nutrition as described above. Extensive convalescence was achieved on the fourth post-operative day, and the animal was taken to the exterior boarding house.

Termination Criteria

1) Significant deterioration in general well-being, in particular, disturbance of eating, 2) Evidence of intra-abdominal abscess, 3) Development of relevant oesophagitis, 4) Evidence of migration of the GORD implant, and 5) Evidence of perforation of the tissue.

Surface Treatments to Improve Tissue Response

The implants were treated with a low pressure (0.3 mBar, 10 min., 90% capacity) oxygen plasma process (TETRA 30 LF PC, Diener electronic GmbH + Co. KG, Nagold, Germany) to enhance the hydrophilicity and cell adhesion, also to allow for the cell ingrowth into the porous inner part of the implant. Further information regarding surface treatment has been reported by Schlicht et al. [43]. The implants were coated with a thin anatase TiO_2 film using a deposition process by GfE Medizintechnik GmbH (GfE Medizintechnik GmbH, Nürnberg, Germany). The surface of the implants

Table 1 Different surface treatments and sterilisation methods

Surface treatment method	Gamma sterilisation	Sample name
Untreated	25 and 60 kGy	Inj. Mould, 25, 60 kGy
Plasma activation	25 and 60 kGy	Inj. Mould, Plasma treating, 25, 60 kGy
Plasma activation	None	Inj. Mould, Plasma treating
TiO_2-deposition	25 and 60 kGy	Inj. Mould, TiO_2-deposition, 25, 60 kGy

Plasma activation and TiO_2-deposition were performed to increase the cytotoxicity of the implants. Gamma sterilisation was carried out for a high sterility assurance level. After these, the implants were tested in vitro and in vivo to determine the influence of the surface treatments and sterilisation on the biocompatibility of the implants

was evenly coated with a thin TiO_2 film on a nanometer scale at low temperature and pressure to protect the bulk properties of the polymer implant. After surface treatment, the implants were sterilised by gamma sterilisation (Isotron, Allershausen, Germany) at 25 and 60 kGy.). The tested implants are listed in Table 1.

Chemical and Physical Analysis After Surface Treatments

A differential scanning calorimeter (DSC, Jupiter Netzsch Gerätebau GmbH, Selb, Germany) was used to determine the melting points, glass transition temperatures and crystallinity of the polymer implants according to the procedure previously described [34].

Molecular weight analysis of the implant was measured according to the procedure previously described [34] in a gel permeation chromatography (GPC) system (600E, Waters GmbH, Eschborn, Germany) with a refractive index detector, Waters 410, a column oven Jetstream, 717 plus Autosampler, three Waters Styragel HT columns 2, 4 and 6.

The attenuated total reflectance Fourier transform infrared spectroscopy (ATR-FTIR; Spectrum One, PerkinElmer Instruments, Rodgau-Juegesheim, Germany) was used to observe the surface structure of the gastric implants after different surface treatments and sterilisation [34].

Characterisation of Macro- and Microstructures After Surface Treatments

MicroCT (SkyScan 1172, SkyScan, Kontich, Belgium) was used to measure the porous structures quantitatively) at 7 µm resolution using a voltage of 59 kV and a current of 167 µA. Image reconstruction and analysis were conducted using the software package provided by SkyScan. The procedure was published elsewhere and, therefore, not further elaborated [30].

Scanning electron microscopy SEM (S-3500 N, Hitachi Science Systems, Tokyo, Japan) was used to observe the cell attachment on the implant surface. In order to observe optical fixation of cell growth on the implant surface with SEM, the sample must be treated by the following procedure. After cell seeding, the implants were washed twice with PBS and immersed in 3% glutaraldehyde (VWR, Darmstadt, Germany) at 4° C for two days. Subsequently, the implants were dehydrated using graded ethanol (VWR, Darmstadt, Germany) series from 50 to 99%, with two ten-minute incubation periods for each step. In the end, dehydration was completed by critical point drying using CO_2 (CO_2 protective gas DIN-32525-C1, Westfalen AG, Münster, Germany). After dehydration, the implants were sputtered and examined in SEM.

The implants were dipped in liquid N_2 after TiO_2-deposition and disrupted manually to expose a fracture for the SEM–EDX testing, which should reveal the deposition quality in the deeper laying pore structure.

In Vitro Experiments After Surface Treatments

A permanent cell line (Detroit 551, CCL-110, ATCC, Manassas, USA) was used in this study, the cultivation of cells used in in vitro experiments in Petri dishes (T25 and T75, TPP, Trasadingen, Switzerland) and the corresponding medium (DMEM, Biochrom AG, Berlin, Germany). A cell culture incubator (Heraeus Kendro Laboratory Products GmbH, Langenselbold, Germany) was used for cell cultivation at 37° C and 5% CO2 atmosphere conditions. A preliminary test was performed using different cell numbers (3000, 5000, 10,000 cells/ml cell suspension) for different cultivation times (3, 5 and 7 days) to determine the 100% confluence of cell proliferation. After testing, it was found that a cell number of 10,000 cells/ml cell suspensions in Petri dish T25 for seven days of cultivation time was the optimal condition for cell cultivation.

Cell vitality was controlled using a microscope (Axiovert 25, Carl Zeiss, Jena, Germany). The Casy® 1-Cell Counter Analyser System, Model TT (Schärfe System GmbH, Reutlingen, Germany), was used to determine the cell number. A weak electrolyte diluted the cell suspension from one hundred (Casy®ton, sterile filtered, Schärfe System GmbH, Reutlingen, Germany) [31]. Vital cells were monitored within a size variant of 10–40 µm. The porous gastric implants were cut to suit the size of 24-Well plates so that buoyancy could be avoided after the insertion of implants into wells. Subsequently, cell suspension with 2×10^5 cells was pipetted onto each sample, and the well plates were placed in a culture incubator (C150, BINDER Inc., Great River, NY, USA) for 60 min at 37 °C under a 5% CO_2 atmosphere. After this, 1 ml medium was added to each sample, and the Well plates were placed in an incubator for further seeding.

WST-1 Assay

Sterile, porous samples (750 mg) from the implant with different surface treatments were incubated in a culture medium for 7 days. The culture medium after incubation (C150, BINDER Inc., Great River, NY, USA) was added to 96-Well plates, and a cell suspension with 6000 cells was given to each well for 1, 3 and 7 days at 37 °C in a 5% CO_2 atmosphere. After a certain incubation time, 10%vol. Cell proliferation reagent WST-1 (Roche diagnostics GmbH, Mannheim, Germany) was added directly into the medium. After 90 min, the behaviour of these fibroblasts was analysed.

Vitality Experiments of the Cultivated Fibroblasts

A LIVE/DEAD® Viability/Cytotoxicity Assay Kit (26611 W, Invitrogen GmbH, Karlsruhe, Germany) with the reagents Calcein AM (4 mM in DMSO) and Ethidiumhomodimer-1 (EthD-1, 2 mM in DMSO/H2O 1:4) was used to test the vitality of the fibroblast in the Gastric implants[44] after 1, 3 and 7 days. The images were recorded with an AxioCam digital camera and assessed with the software AxioVision 4.6 (Carl Zeiss, Jena, Germany) [45].

Second Animal Experiment (Rabbit Study) to Verify Tissue Ingrowth

The second in vivo test on rabbits served as a model of cells ingrowth into the porous structure prior to a second large pig study. The implant was cut into pieces and subcutaneously implanted in the dorsal region of New Zealand white female rabbits (Mean weight 3.01 ± 0.11 kg) and left to heal for 12 and 24 weeks. The test plan is shown in * MERGEFORMAT Fig. 10. Three healthy adults New Zealand white rabbits for each implantation period were operated on, i.e. 12 pieces of each implant type for every implantation time were available. Operation time was $40.75 \text{ min} \pm 17.8$. The rabbits were housed in single cages with a base area of 0.4 m^2 and unlimited water and food according to the European guideline (2007/526/EG). The German Animal Research Authority approved the experiments and registered this authority. The procedures were conducted in accordance with the European Animal Welfare Act of December 20th, 1974, No. 73, Chapter VI, Sects. 20–22, and the German Regulation on Animal Experimentation of October 16th 1996. The persons who performed the surgical procedure were trained to obey animal welfare and handling protocols.

At the end of each implantation period, all pieces of implants were explanted for further histological analysis. Due to the flexibility and porous structure of Gastric implants, the histological preparation of implants with tissue based on paraffin wax embedding was unsuitable. Thus the histological preparation was made using cold polymerisation of PMMA (poly-methylmethacrylate) [46]. Paragon-colouring was used for the identification of cells as well as tissue from implants. The preparations were observed using light microscopy (Axiovert 200, Carl Zeiss, Jena, Germany). In addition, two independent pathologists did the histopathological scoring of the slides.

Statistical Analysis

The results were expressed as means with standard errors. One-way ANOVA then analysed the data, and the post hoc paired Tukey test (Origin 7, OriginLab Corporation, Northampton, USA). All p values were compared with a value of 0.05 to determine significance. The results presented in this article are significant unless otherwise stated.

Results and Discussion

First Animal Study

Pigs were selected as animal model due to their anatomy similarity to human oesophagus and stomach. The series of animal experiments was initially started with six pigs of this breed. The laparoscopic device implanted the GORD implant (Fig. 1, A-F). It was already known that the GORD implant had a high potential for inducing stenosis, and the pigs would live for less than a year. The domestic pigs were sacrificed after an average of 135 days (22–273 days) in 4 cases (70–273 days) due to poor general conditions attributed to oesophageal stenosis. One pig had a wound-healing disorder requiring euthanasia at 22 days (Fig. 1 G). In one pig, the implant dislocated into the thorax, which meant no signs of an eating disorder until euthanasia after 226 days (Fig. 1 G). The implant could not be localised in vivo because the GORD implant was not radiopaque.

In summary, it can be stated that the GORD implant was still at the site of implantation after more than 42 days in only one of 14 test animals (7%) without causing oesophagal stenosis. In this case, however, the implant was not fixed but lay loosely around the oesophagus. In all explants, the capsular tissue was easily detached from the implant, suggesting that the desired tissue from the oesophageal wall did not penetrate the implant's porous (Fig. 1, H). Therefore, a fixation as a hypothesis was not achieved. After implantation in pigs, the implant was encased in a capsule. This process did not end but progressed—sometimes slowly, sometimes faster—until the oesophagus was closed by the constricting scar tissue (Fig. 1, I). This condition was reached in some pigs after two months, in others only after nine months. Histological analysis showed no ingrowth of fibroblast or any other connective tissue into the porous part of the implant, a hypothesis (Fig. 1, I, white arrow), which is likely to be linked to polymer hydrophobicity [47–50].

The reasons for the unsatisfactory results of GORD's implant in animal experiments (Fig. 1) were determined:

- The implant was not sufficiently fixed at the site of implantation.
- The GORD implant's porous inner side was **not infiltrated** by any biological tissue (Fig. 1, I).
- Hydrophobic properties of the polyurethane prevent the cells of the oesophageal wall from initially coming into contact with deeper pores and, thus, from growing.
- Sharp edges lead to severe irritation of the surrounding tissue and thus to increased scar tissue.

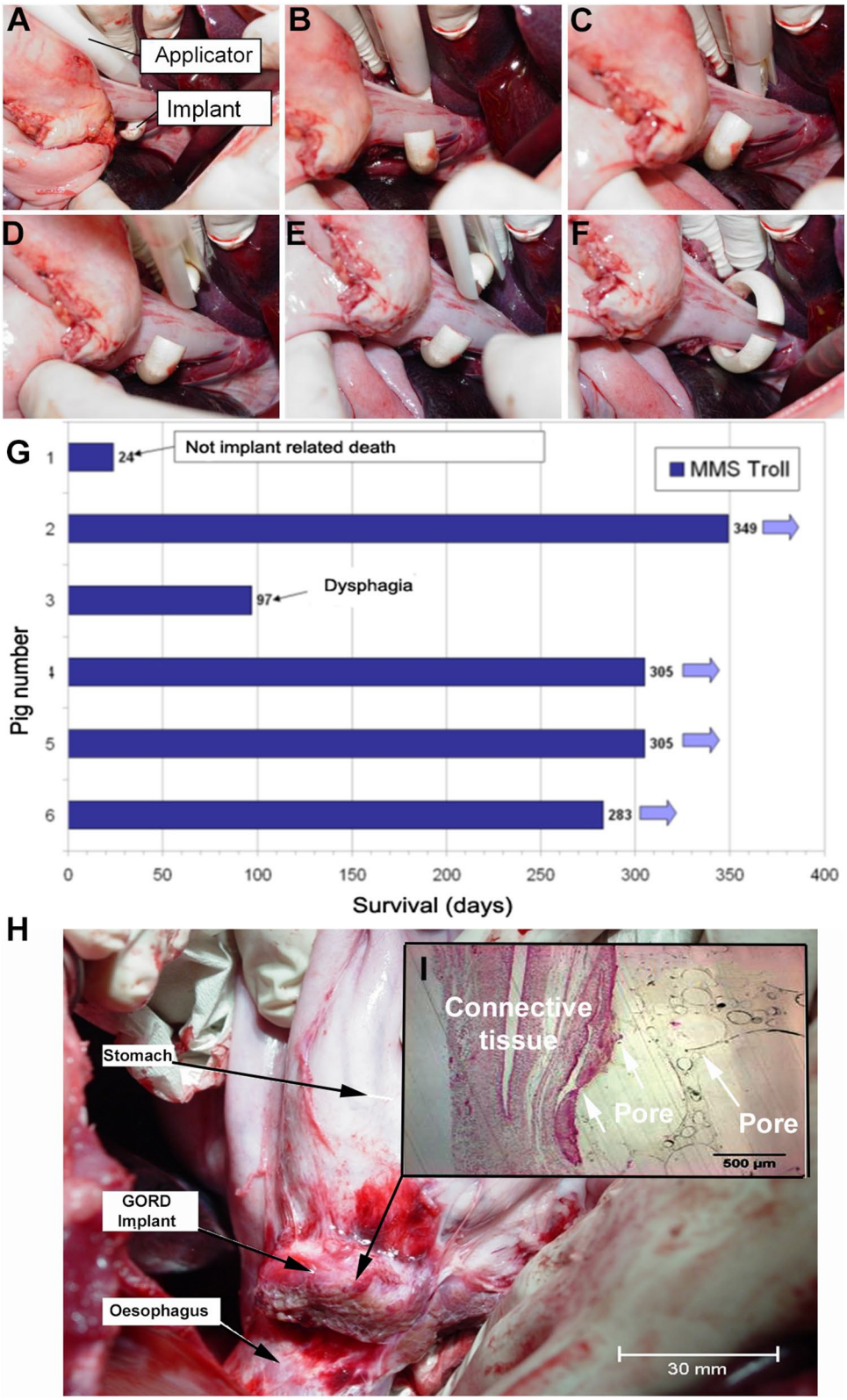

Fig. 1 Frist animal trial of the GORD implant, where the applicator was used to place the implant around the pig's oesophagus (**A**–**F**). The long-term pig study ($n=6$) had to be terminated due to uncontrolled encapsulation of the implant (**H**), which resulted in dysphagia and no intact food. Histological evidence showed no ingrowth of fibrous or any other tissues into the porous structure (**I**), where the connective tissue did not reach the porous section of the implant (white arrows). This lead to migration of the implant along the oesophagus, an unwanted event as the implant should stay fixated at the LOS

- The implant was not visible on X-rays, which means that the position of the implant must be checked postoperatively difficult.

Due to an unsatisfactory pig study, the implant design was modified (Fig. 2), where the gastric implant was made thinner, reduced sharp edges and a nitinol ring was placed

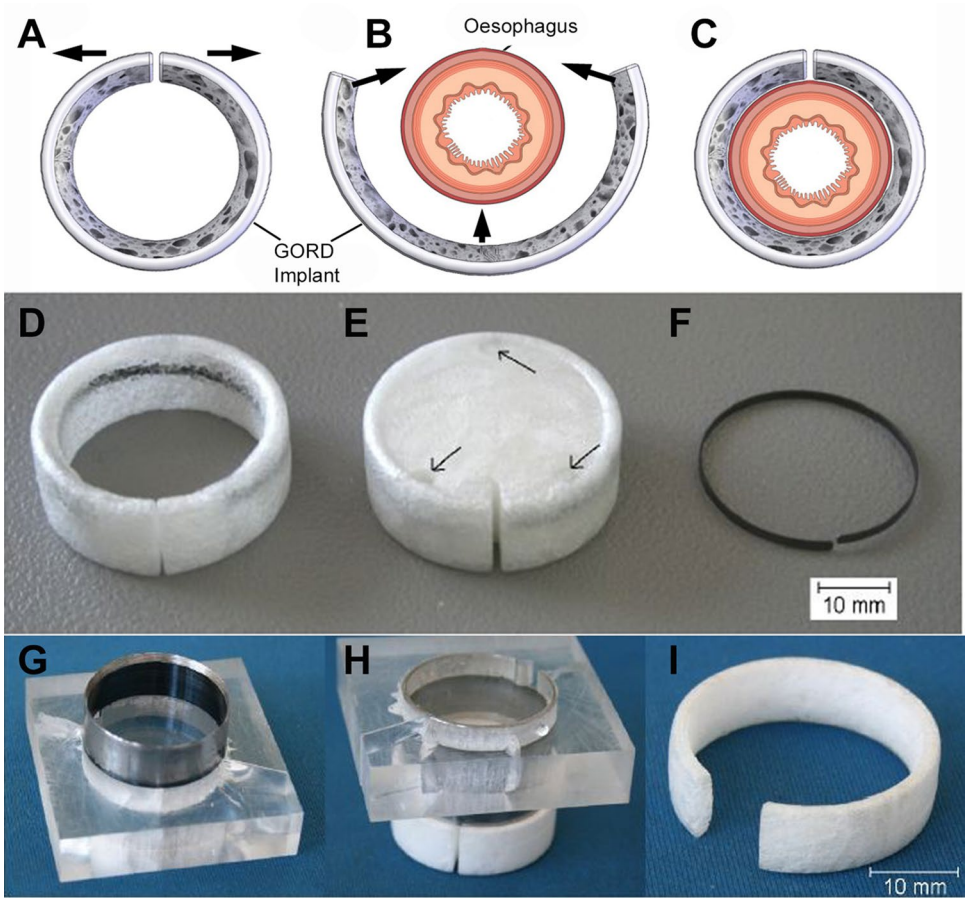

Fig. 2 Improvement to the gastric implant after the pig study. Thinner implants were developed with less sharp edges to reduce encapsulation (**A**–**C**). The implant was injected moulded cylinder (**D**) to ensure an even porous structure. The innerside was removed by a custom-made stamp (**G** and **H**). One can see the outside closed pore structure and the inside porous structure (**I**) after the innerside was removed. The gastric implant was inserted with a Nitinol wire (**D**) such that the implant could exert pressure on the LOS to reduce the sphincter volume, as shown in A-C. The nitinol ring not only exerts pressure but also enable post-operative inspection of the implant as the metal is more easily recognised by, e.g. ultrasound, MRI, CT or X-ray

inside the implant. The nitinol ring should extend additional pressure to the LOS for more effective closure of the sphincter as well as enable post-operative inspection by imaging techniques (ultrasound, X-ray, Magnetic resonance imaging (MRI), computerised tomography (CT), etc.). In addition, two surface treatments based on literature were chosen [49, 50].

Surface Modification to GORD Implant to Improve Biological Response

The biocompatibility of an implant is decided on its properties facilitated by its surface properties and/or the combination of chemical, physical, biological, and mechanical properties [51, 52]. One major disadvantage of polyurethanes is their hydrophobicity [48, 53], which may inhibit cell attachment, spread and growth [54]. One-way is to use a low-powered plasma treatment with low reaction temperature, which chemically changes the polymeric surface [55, 56]. Alves et al. found that the plasma treatment process on polyurethane increased the hydrophilicity [51]. In addition, several research groups have investigated improving cell attachment on such polymeric surfaces [57–61]. Plasma activation and TiO_2 deposition were utilised as a surface treatment to improve cell adhesion and aid tissue ingrowth into the implant [62]. Gamma irradiation was used as the sterilisation method since this sterilisation method has been reported to be favourable for this kind of thermoplastic polyurethane as opposed to steam sterilisation [32, 34].

Pore Morphology

The pore morphology was analysed with microCT, where five different sections of the porous structure were chosen. The mean porosity was found to be $81.4 \pm 0.4\%$, mean pore size 264 ± 64.0 µm and strut size 43.4 µm (Table 2). According to previous studies, this pore structure should allow for tissue ingrowth [63–65]. The degree of anisotropy was 1.41, indicating that the pores were nearly circular [66]. There were no significant differences between the different surface treatments (Table 2).

Chemical Changes of Implants After Surface Treatments and Sterilisation

The gastric implants' chemical state after different treatments were qualitatively characterised through ATR FT-IR (Annotated Transmission Reflection Fourier Transmission

Table 2 Selected parameters from 3D µCT analysis displaying mean values and standard deviation (SD) from selected area of the porous gastric implant ($n=3$)

	Parameter	Mean	SD
Inj. Mould. 25 kGy	Porosity (%)	81.4	0.4
	Object surface (µm2)	435,784,219.0	7,549,024.0
	Intersection surface (µm2/µm3)	39,576,397.5	983,133.5
	Mean pore size (µm)	263.8	64.1
	Structure separation (µm)	43.4	1.0
	Degree of anisotropy	1.4	0.2
	Fractal dimension	2.4	0.0
Inj. Mould. Plasma treating, 25 kGy	Porosity (%)	82.3	0.4
	Object surface (µm2)	441,013,629.6	7,639,612.3
	Intersection surface (µm2/µm3)	40,047,266.2	992,407.1
	Mean pore size (µm)	266.9	64.8
	Structure separation (µm)	44.0	1.2
	Degree of anisotropy	1.4	0.2
	Fractal dimension	2.4	0.0
Inj. Mould. TiO2 deposition, 25 kGy	Porosity (%)	81.1	0.4
	Object surface (µm2)	434,476,866.3	7,526,376.9
	Intersection surface (µm2/µm3)	39,455,680.3	978,190.1
	Mean pore size (µm)	263.2	63.9
	Structure separation (µm)	43.3	1.0
	Degree of anisotropy	1.4	0.2
	Fractal dimension	2.4	0.0

No significant difference between groups

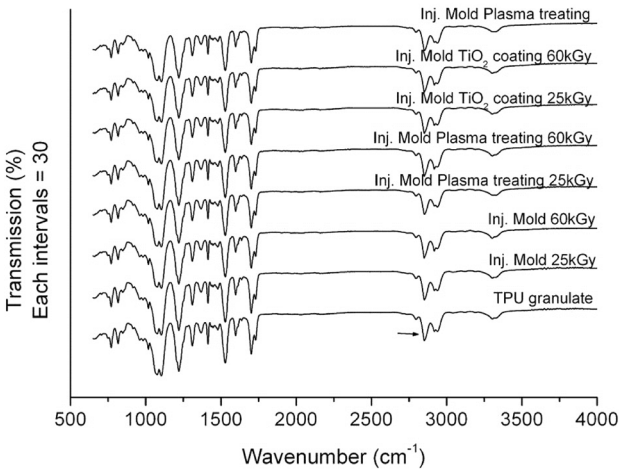

Fig. 3 ATR FT-IR-spectra of implants following different implant surface treatments and sterilisation

Table 3 Weight average molecular mass (Mw) of the gastric implants

Sample	M_w (g/mol)	SD
Unprocessed TPU	226,239.6	3926.4
Inj. Mould, non-sterile	109,321.8[a,]	237.7
Inj. Mould. 25 kGy	128,056.8 [a,b]	730.7
Inj. Mould. 60 kGy	152,307.8 [a,b,c]	2181.3
Inj. Mould. Plasma treated	111,634.8 [a,]	3275.3
Inj. Mould. Plasma treating, 25 kGy	122,226.3 [a,b]	593.3
Inj. Mould. Plasma treating, 60 kGy	152,663.0 [a,b,c]	1624.3
Inj. Mould. TiO2 deposition	120,253.9 [a,b]	261.4
Inj. Mould. TiO2 deposition, 25 kGy	140,862.5 [a,b]	803.7
Inj. Mould. TiO2 deposition, 60 kGy	161,446.3 [a,b]	2312.1

[a]$p<0.05$ versus unprocessed thermoplastic polyurethane TPU, [b]$p<0.05$ versus Inj. Mould, non-sterile, [c]$p<0.05$ versus Inj. Mould, 25 kGy, Inj. Mould, $n=6$, *Inj. Mould* injection moulded

Infrared Analysis) (* MERGEFORMAT Fig. 3). No major difference in the spectra was detected (< 5% transmission deviation). Plasma activation, TiO_2-deposition and different gamma-ray doses had only minor alterations to the implant surface chemistry. Similar results were also presented in a similar study [33, 67].

Contact angle and water adsorption test with and without surface treatments are presented in Table 3. After surface treatments, the contact angle has decreased from 103° for untreated to 64° for plasma-activated and 78° for TiO_2-deposition. However, the contact angle measurement was performed on the injection moulded plate due to the difficulty of measuring the contact angle on a porous surface. The contact angle reduction induced by plasma activation can be attributed to surface functionalisation by interlock polar groups such as (−C−O−C) and (−C=O) [68, 69]. TiO_2-deposition increases polar group (such as −Ti−O−)

due to its chemical structure. At the same time, potential oxidation of the polymer surface during the deposition process may also lead to the rise of polar species [70–72]. The porous implant surface was treated by plasma activation, and TiO_2-deposition adsorbed the water faster than the untreated surface. Since studies have shown that one can achieve higher cell adhesion by lowering the material surface's water contact angle by more than seventy degrees [73–75], the current treatment should positively affect the cell response towards the GORD implant.

Since the implant used is highly porous (> 80%) and has large pore diameters (mean size 264 µm), we were interested in the penetration depth of the TiO_2-deposition. The distribution of titanium atoms was analysed with SEM–EDX (Energy Dispersive X-ray Spectroscopy) and showed that these atoms could be found as deep as 3 mm inside the implant (Fig. 4). As a result, the concentration of titanium atoms decreased in depth.

The thermal analysis showed that the γ-sterilized implants had three peaks (Fig. 5). The first and second peaks (ca. 70 °C, 115 °C) came from the short- and long-range disruption order chains. The third peak (ca. 175 °C) can be attributed to the melting of the microcrystalline region in the hard segment microphase [76]. Unprocessed thermoplastic polyurethane had only two inconspicuous peaks. Since the peak area was directly proportional to the crystallinity of polymers, the peak changes may indicate the processing and sterilisation influences on the gastric implant structure as the implant's crystallinity significantly increased after the injection moulding compared with unprocessed thermoplastic polyurethane. The increased orientation degree of thermoplastic polyurethane long molecule chains has been

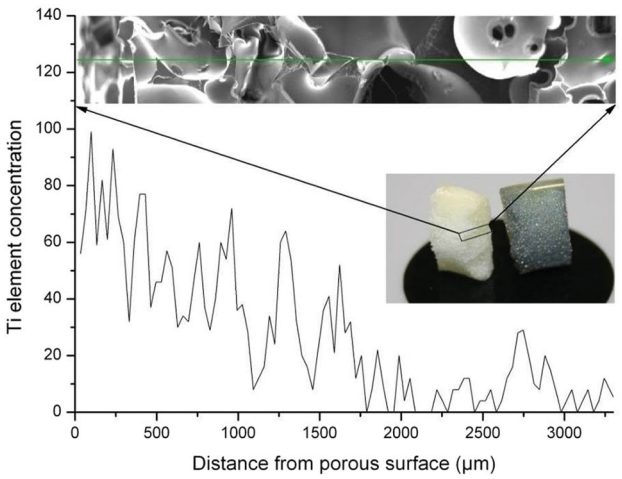

Fig. 4 The Ti-atom distribution on the fracture of the implant after TiO2 deposition. The observed fracture of the implant is shown in the figure. The right half part was coated with gold. It is seen that from left to right, the Ti-atom concentration has decreased continuously. The Ti-atom was found even 3 mm deep inside the implant

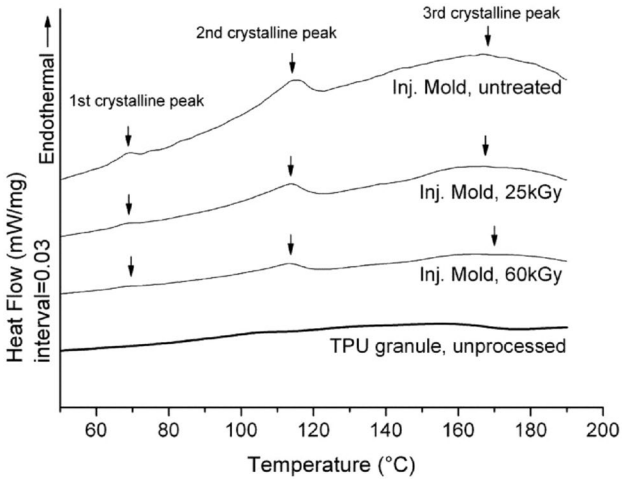

Fig. 5 Differential Scanning Calorimeter (DSC) analysis of implants after gamma-ray sterilisation

reported previously due to the shearing and heat [77]. As reported by others, gamma radiation causes crosslinking of long polymer chains, where there is a limiting chain's free motion, and therefore prohibited crystallite regions [78, 79]. As a result, the implant's crystallinity by 25 kGy showed a reduction according to the smaller peak area compared with the unsterilised gastric implant, and the lowest value was by 60 kGy due to more crosslinking of polymer long chains.

Finally, the weight average molar mass of the gastric implant was tested in this study (Table 3). Many physical properties of polymers has related to the molar mass, such as the rheological properties of the polymer melt [80]. Some chemical structure changes in the polymer can be observed by measuring the molar mass of the polymer [81, 82]. Consequently, the degradation of polymers can be proved if the molar mass has changed due to the breaking of the long-chain molecule [83–85]. Table 3 shows the molar mass of the gastric implants with or without surface treatments and gamma sterilisations. The unprocessed thermoplastic polyurethane has the largest molar mass, $M_{w,}$ of 226 kg/mol. After 4 h of hot air drying, a small loss of M_w (approx. 5%) was observed. After injection moulding, the M_w decreased quickly to the value of 109 kg/mol, and almost half of the thermoplastic polyurethane granules were unprocessed. The molar mass loss of polymers due to the processing was widely found in most polymers[86, 87]. The molar mass loss of thermoplastic polyurethane due to injection moulding was also found in different studies [88, 89]. The general agreement was that the polymer processing methods, such as extrusion and injection moulding, stress the polymer long chain due to the high temperature, high pressure in the cylinder, and the shearing of the screws. Those factors break the polymers' long molecule chain and the consequent molar mass loss [90, 91].

The gastric implants irradiated by gamma-rays behaved reversely and gained molar mass. The M_w of implant for 25 kGy and 60 kGy irradiation was 128 kg/mol, 152 kg/mol, 17% and 39% improvement, respectively. Gamma-ray irradiation is widely used for inducing a crosslinking between free monomers or short polymer chains to control the mechanical properties of polymers [92–94]. It could be assumed that the thermoplastic polyurethane molecule chain's crosslinking has occurred due to gamma-ray irradiation. One of the results of gamma-ray irradiation is the rise of molar mass. Similar observations were found for PU [95, 96], but reverse results were also reported [97, 98]. It seemed that at a low dose range of radiation, the molar mass increases with rises in the dose but acts on the contrary at a high dose range of radiation.

The two surface treatments did not alter the gastric implant's molecular weight, as no significant differences were seen between these two groups (plasma-treated versus TiO2 deposition) for Mw (Table 3).

All tests mentioned above have indicated that the surface treatments and gamma-ray sterilisation have changed the surface properties of thermoplastic polyurethane foamed implants on a micro-scale and the physical characteristics of thermoplastic polyurethane itself. These changes are expected for the change biocompatibility of the implants. The following sections will describe the biological tests and the influence of surface treatments and sterilisations on the implants (Fig. 6).

In Vitro Study to Verify the Potential of Surface Treatments

The Influences of Surface Treatments

The implants after surface treatments showed a higher optical density on each test day than implants without treatment, and all results were consistent with the changes in the wettability of the implants after surface treatments (Fig. 7, A). The optical density was directly proportional to the number of viable cells, which indicated that the surface treatments such as plasma activation or TiO_2-deposition could effectively improve the implant cytotoxicity. Similar results have been verified by others [56, 99]. For example, on days 1, 3 and 7 after cell seeding, the optical density of every sample type had a durative increase, which meant appropriate cell proliferation. All implants showed optical density values over 70% of the values of negative controls, which meant that the implants were non-cytotoxic [100].

A cell vitality colouring test, LIVE/DEAD® was performed as the qualitative test of the cell response of implants (Fig. 7). LIVE/DEAD® confirmed the WST-1 assay. The untreated sample showed the lowest cell vitality, fewer vital cells and more nuclei of non-vital cells (Fig. 8, A), whereas higher cell vitality levels (more green vital cells) were found in implants after plasma activation and TiO_2-deposition (Fig. 8, D and G). In addition, cells' netlike morphology was found in implants' tests after surface treatments. The increase of optical density in WST-1 assay and vitality of cells in LIVE/DEAD® colouring assay could primarily be attributed to the modified surface of implants induced by plasma activation and sterilisation, which efficiently prevented the release of toxic degradation products. Methylenedianiline (MDA) was the main toxic degradation product released from thermoplastic polyurethane [32, 101]. The results showed a slight cytotoxic effect of implants after surface treatment.

The proliferation of cells on the implant surface was tested through cell seeding and is shown in Fig. 9. After 7 days of incubation, all implants were attached by seeded cells. The untreated implant surface was slightly covered by cells (Fig. 9A and B). On the contrary, a cell layer completely covered the implant surface with treatments (plasma

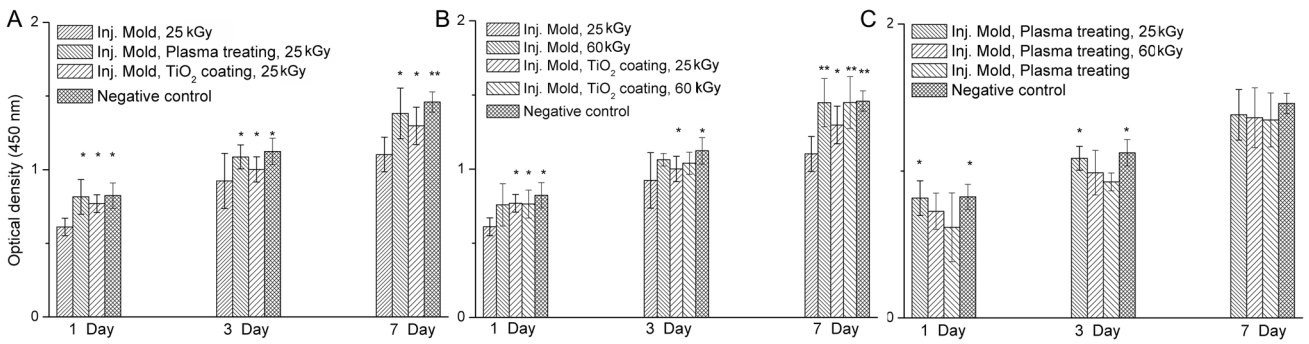

Fig. 6 WST-1 assays to compare the mitochondrial activities of fibroblast on implant surface with different surface treatments (**A**), different gamma-ray irradiation (**B**), and effects of gamma-ray irradiation on the plasma-treated implant (**C**). The negative control was pure medium. The tests were performed on the 1st, 3rd and 7th day after cell seeding to indicate the proliferation of cells on the implant surface. The optical density is directly proportional to the number of viable cells. (*$p < 0.05$, **$p < 0.05$ vs. implants without surface treatments at the same testing day, $n = 8$)

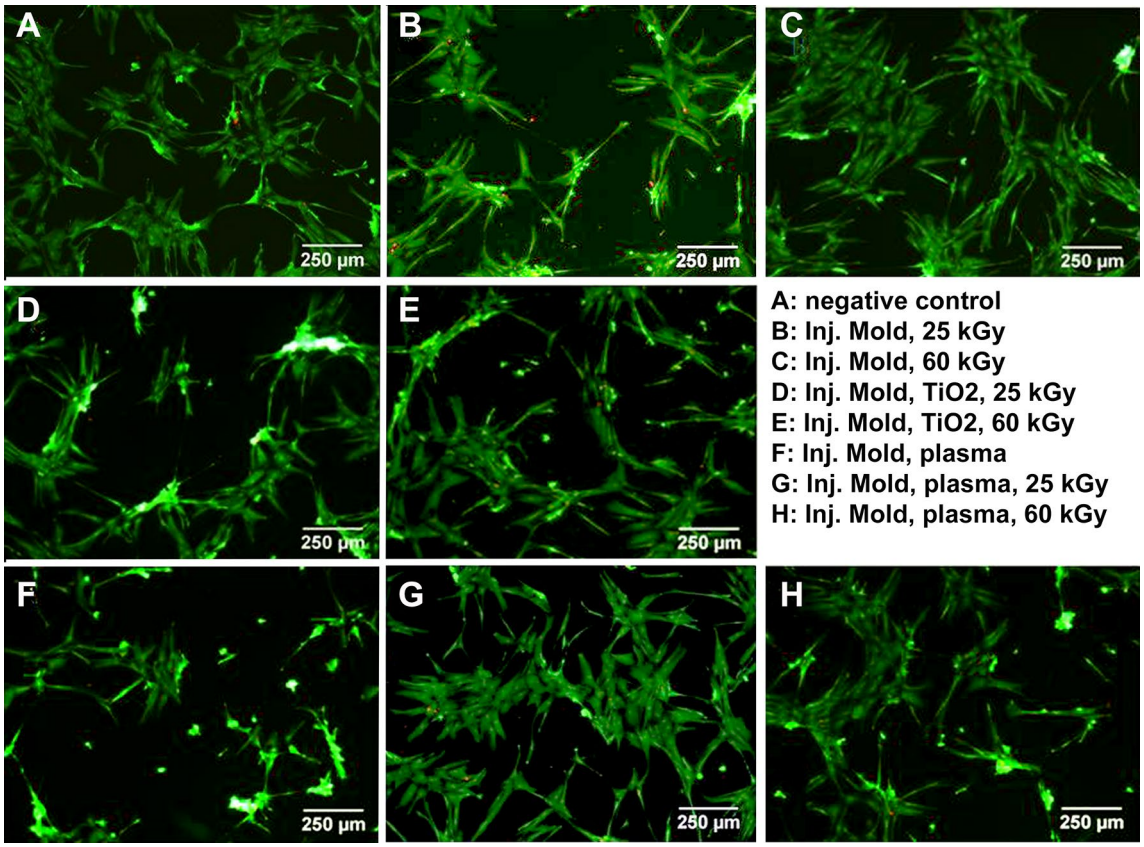

Fig. 7 Vitality colouring (LIVE/DEAD®) after cultivation of fibroblastic cell with extract medium. **A**: negative control; **B**: implant sterilised at 25 kGy; **C**: implant sterilised at 25 kGy, **D**: Implant with TiO_2-deposition and sterilised at 25 kGy; **E**: Implant with TiO_2-deposition and sterilised at 25 kGy; **F**: Implant with plasma deposition and no sterilisation; **G**: Implant with plasma deposition and sterilised at 25 kGy; **H**: Implant with plasma deposition and sterilised at 60 kGy. Green is vital cells, and red is the nuclei of non-vital cells. The images were taken after three days of incubation

activation and TiO2-deposition) (Fig. 9C-F). The cells attached themselves to the implant surface, some even into the porous structure. This ingrowth of cells into the pore was desired because it could prevent the migration of implants along the oesophagus. A significant acceleration of the cell adhesion and proliferation was observed due to the surface treatment (Fig. 9C-F). The cell seeding results could suggest that the hydrophilic implant surface after the plasma treatment and TiO_2-deposition was more favourable for the cell spreading and growth than the hydrophobic surface of the untreated implant. Consequently, oxygen atoms or radicals improved the cell spreading and proliferation behaviours on polymeric surfaces, as also seen by Filova et al. [102].

The Influences of Gamma-Ray Irradiation as a Sterilisation Method

All the implants were sterilised through gamma-ray irradiation before WST-1 assay was performed. In this case, two different doses of irradiation were tested on the implant to understand the potential effects of gamma-ray irradiation on the surface properties after treatment, as well as the biological behaviours of implants. The WST-1 assay of extract of untreated and TiO_2-coated implants with different gamma-ray irradiation doses is illustrated in Fig. 7, B. The tests of plasma-treated implants will be separately discussed. The optical density of the untreated implant increased significantly with an increasing dose of gamma-ray irradiation on every test day. The reason could be a change in the chemical structure of thermoplastic polyurethane after the irradiation. It was assumed that the crosslinking of the thermoplastic polyurethane molecule chain had occurred due to the gamma-ray irradiation, and the release of toxic degradation product from implants was consequently prevented. As a result, optical density with increased gamma-ray dose was observed. The increase in optical density of TiO_2-coated implants from 25 to 60 kGy gamma-ray irradiation could also be explained by the same reason. For example, the TiO_2-layer coated on the implant surface may have acted as a protection layer to prevent the release of toxic degradation products so that the TiO_2-coated implant at 25 kGy of gamma-ray always had a higher optical density than those

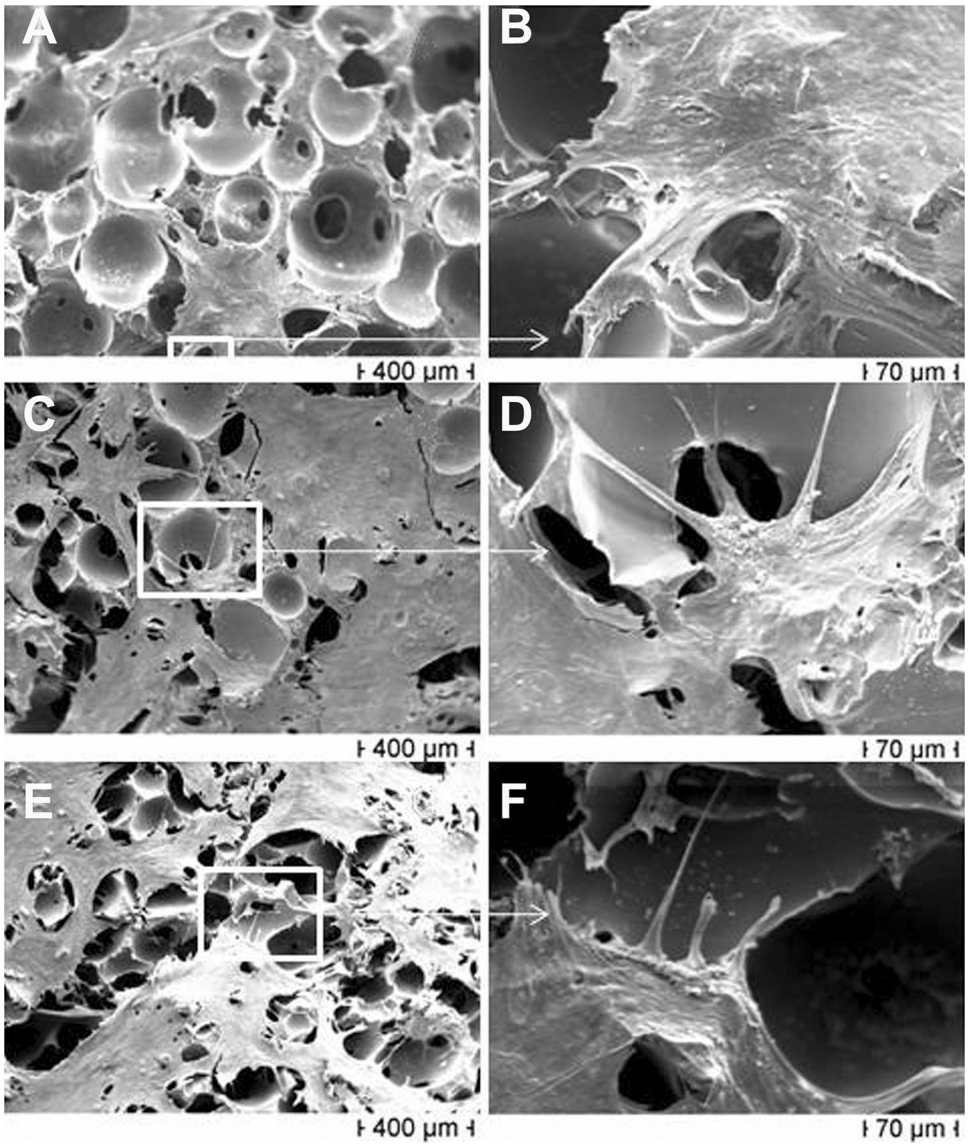

Fig. 8 SEM images of the implant surface with/without treatment after 7-day incubation. **A** and **B**: Untreated sample; **C** and **D**: Sample after plasma activation; **E** and **F**: Sample after TiO_2-deposition. All implants were sterilised with a 25 kGy gamma-ray

without treatment. All implants showed an optical density over 70% of negative control and indicated adequate cell mitochondrial activity.

The LIVE/DEAD® assay tests (Fig. 8) gave qualitatively similar results to WST-1 assays. The untreated sample with 25 kGy of gamma-ray irradiation showed the worst cell vitality (Fig. 8, B). However, with the rise of the gamma-ray dose, more viable cells were found (Fig. 8, C); this effect was not obvious for TiO_2-coated implants (Fig. 8, D and E).

After seven days of incubation, the cells have well proliferated on the TiO_2-coated surface of implants (Fig. 10). Both gamma-ray doses found a homogeneous cell layer, and no apparent difference in cell proliferation was observed (Fig. 10, C and D). Untreated implants showed few cells on their surface (Fig. 10, A and B). The cells spread heterogeneously and just partially covered the implant surfaces. However, all implants showed ingrowth of cells into the porous structure, especially for the TiO_2-coated implants (Fig. 10, C and D).

Figure 7, C demonstrated the WST-1 assay of implants treated by plasma activation with and without sterilisation. The optical density of unsterilised implants had the lowest value. The reason could be attributed to the plasma treatment's inadequacy of the sterilisation process, although efficacy has been reported [103–105]. The implants, after sterilisation, showed a higher optical density on every test day. The rise of irradiation doses from 25 to 60 kGy lead to a reduction of optical density. This change was clear on the 1st and 3rd test days but not significant on day 7. The reduction of optical density with the increased irradiation dose was due to the changes in the chemical structure of the modified implant surface [95]. This change could destroy the formed layer induced by plasma activation on the surface of implants and reduce the plasma activation's positive effect

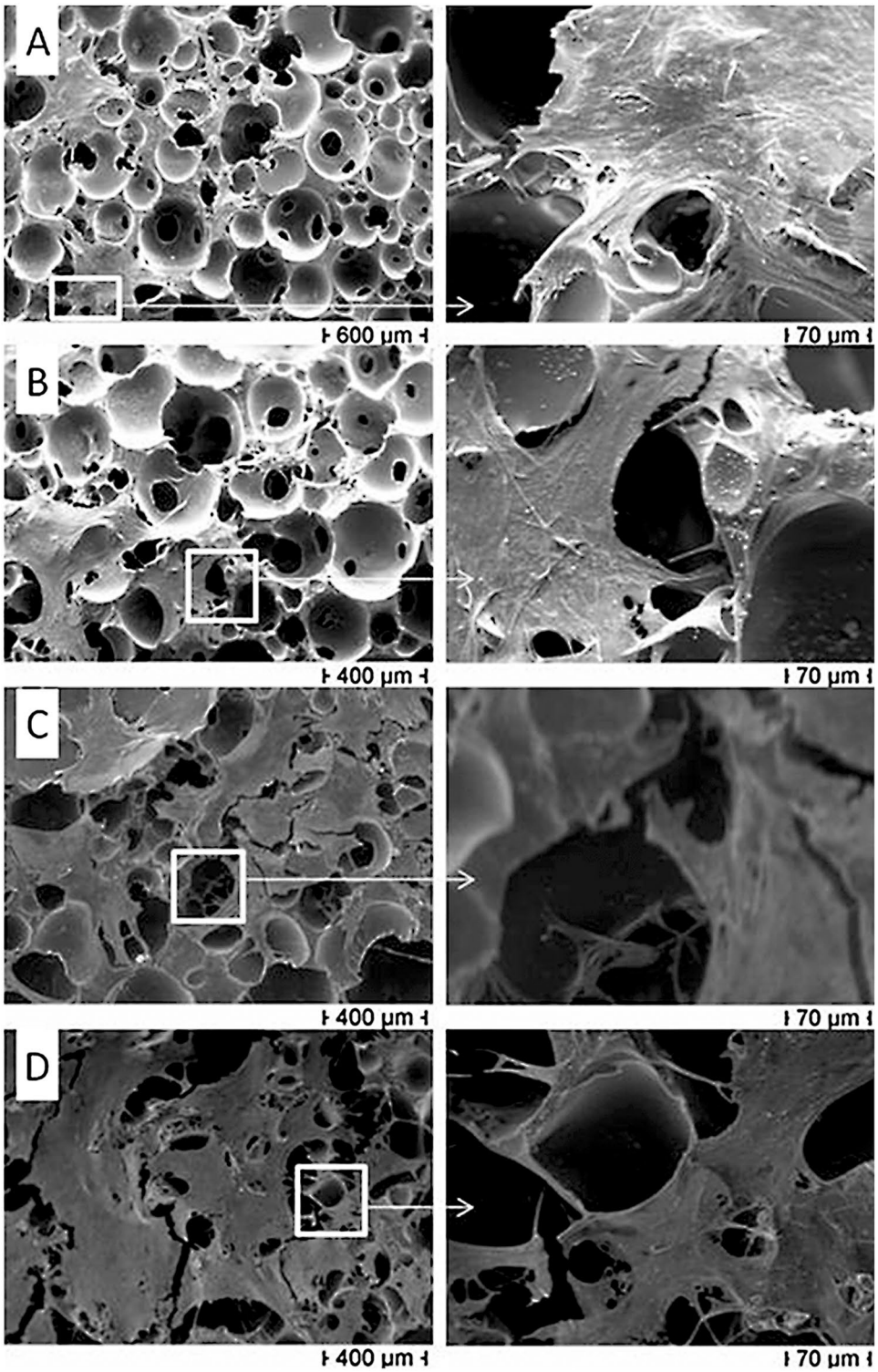

Fig. 9 SEM images of the surface of the implant with different gamma-ray doses after seven days of incubation. A and B are untreated implants with 25 and 60 kGy gamma-ray, C and D are TiO_2-coated implants with 25 and 60 kGy gamma-ray

on the implant's biological behaviour. Table 3 indicated that the percentage of the oxygen element of the implant surface was changed after gamma-ray irradiation. The oxygen content has increased from $29.7 \pm 0.2\%$ to $36.6 \pm 7.11\%$ after 25 kGy irradiation. More irradiation leads to a slight decrease in this value. The significant deviation change at 25 kGy irradiation indicated a less homogeneous oxygen distribution on the implant surface, which could partly prove the present chemical structure changes on the modified implant surface. The exact reaction induced by irradiation was not clear. However, changes in the chemical structure of the implant were verified. This change, maybe damage, of

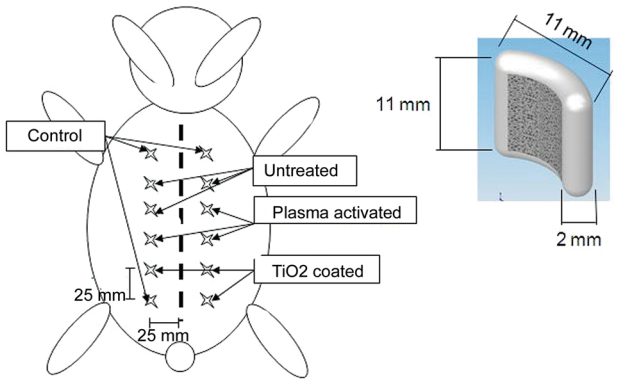

Fig. 10 Test plan for second in vivo study on rabbit showing the positioning of the specimen. 12 pieces of the implant were implanted under the skin of the back of the rabbit. 4 of 12 are PE without porous structure as control, 4 untreated, 4 with plasma treatment and 4 with TiO_2-deposition. For each implantation time, there were three rabbits available

the formed layer induced by plasma activation could lead to more release of toxic degradation product and lower optical density with the rise of irradiation dose.

The LIVE/DEAD® assay tests were consistent with the results of the WST-1 assays (Fig. 8, F–H). The unsterilised implant showed that the worst case of the vitality of cells might be due to its unsterilised state (Fig. 8, F). The implants, after sterilisation, have shown better cell vitality (Fig. 8, G-H).

Second In Vivo Tests to Verify Tissue Ingrowth Due to Surface Treatments

After in vitro tests, the implant should be tested in vivo to indicate its functionality and biocompatibility. In this study, the implant was first tested on New Zealand White rabbits to prove the hypothesis of cell ingrowth and biocompatibility of the gastric implants. All operated rabbits were healthy during the entire implantation period (24 weeks). No distinctive signs of inflammation or infection in any surviving animals were found. During the experiments, the average weight of the rabbits was 3.01 ± 0.11 kg. The histological micrographs of implants after two weeks of embedding time are shown in * MERGEFORMAT Fig. 11. All implants were fully encapsulated by a fibrous connective tissue induced due to the cellular response. The thickness of a capsule varied from 200 µm to 800 µm. The untreated implant showed no ingrowth of tissues and cells into the porous structure of implants, whereas the plasma-activated implant induced an obvious ingrowth of tissue and cells. The TiO_2-coated implant showed just some ingrowth of tissues but less than in plasma-activated implants (Table 4).

After 24 weeks, the capsule thickness around the implants decreased for all three groups, maximal 200 µm. A capsule decrease from the gastric implant would the clinical performance since it would reduce the dysphagia as pigs suffered from dysphagia due to uncontrolled implant encapsulation from the first animal trial. The ingrowth of tissues and

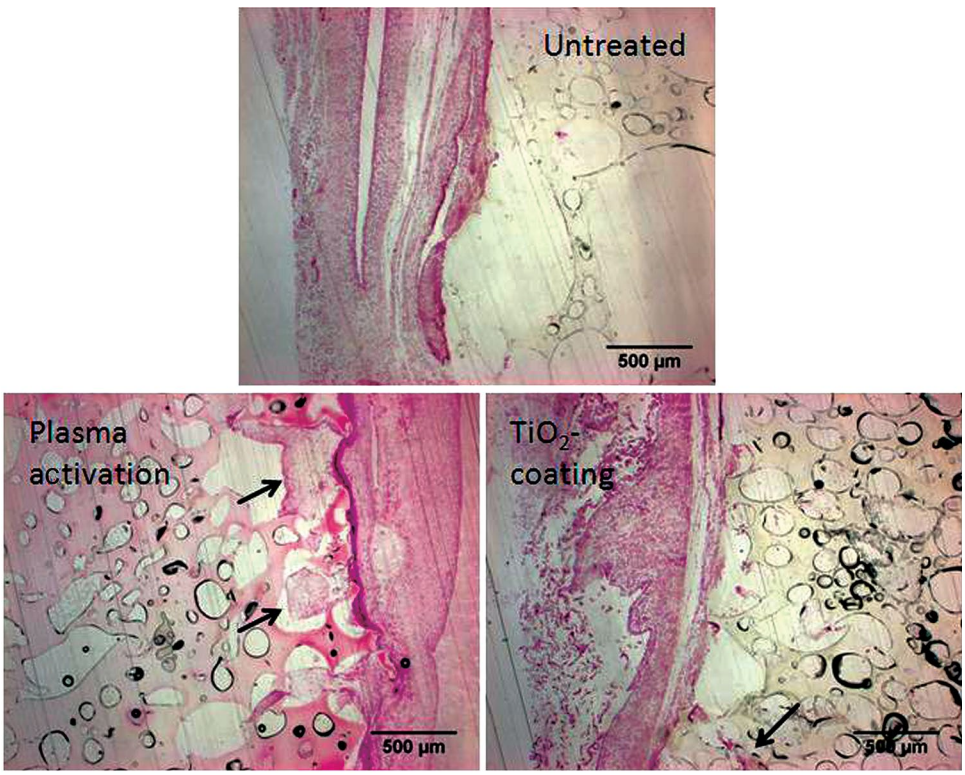

Fig. 11 Histological micrographs of implants after two weeks embedding time. The red region represents the fibrous tissue outside the implants. The black arrow marked the tissue and cells that have grown into the implants' porous structure. The black areas were contaminations during the sample preparation

Table 4 Histopathological scoring of the histological slides ($n = 20$) from the second in vivo experiment

	Control (Implant of PE)		GORD implant-No surface treatment		GORD implant-Plasma-treated		GORD implant-TiO_2 treated	
	12 W	24 W	12 W	24 W	12 W	24 W	12 W	24 W
Encapsulation around the implant	Yes	Yes	Yes	Yes	Yes	Yes	Yes	Yes
Tissue ingrowth into the porous structure	0	0	+	+	+ + +	+ + +	+ +	+ +
Tissue in growth in the entire porous structure	No	No	No	No	No	Almost	No	No

0 no sign, + some cellular structure, + + several cellular layers, + + + complete tissue ingrowth

cells has strongly increased by plasma-activated implants, and the TiO_2-coated implants showed less ingrowth (* MERGEFORMAT Fig. 12). In the case of plasma-activated and untreated implants, the tissue has grown almost 1 mm deep into the implant. Some cells were even found in the middle of the implant (Table 4). Considering the fibrous capsule and cell ingrowth, the aim of fixing the implant around the oesophagus's sphincter through cell ingrowth could be achieved. Previous study has shown that fibroblastic ingrowth into biomaterial, can fixate devices in soft tissues [106–109]. Lehle et al. found that after 4 weeks, the implants made of PET and PP, uncoated and TiO_2-coated, showed a thinner capsule compared with results from 1 week of implantation in rats [110]. The histocompatibility of TiO_2-coated implants was worse than plasma treated, even untreated, whereas, in an earlier study of in vitro tests with human fibroblast, the TiO_2-coated implants always had comparable cytotoxicity to plasma-treated implants and better than untreated implants (Table 4). On the other hand, it was reported that an increased foreign body giant cell density and thick collagen bundles around TiO_2-coated implant compared with uncoated controls were observed in tests on rabbits [111]. This may be the reason for less histocompatibility of TiO_2-coated implants or enhanced in vivo degradation due to the TiO_2 deposition process. On the other side, the tissue reactions depend on many aspects such as surface properties, dimension and nature of the implant, which is relevant [112].

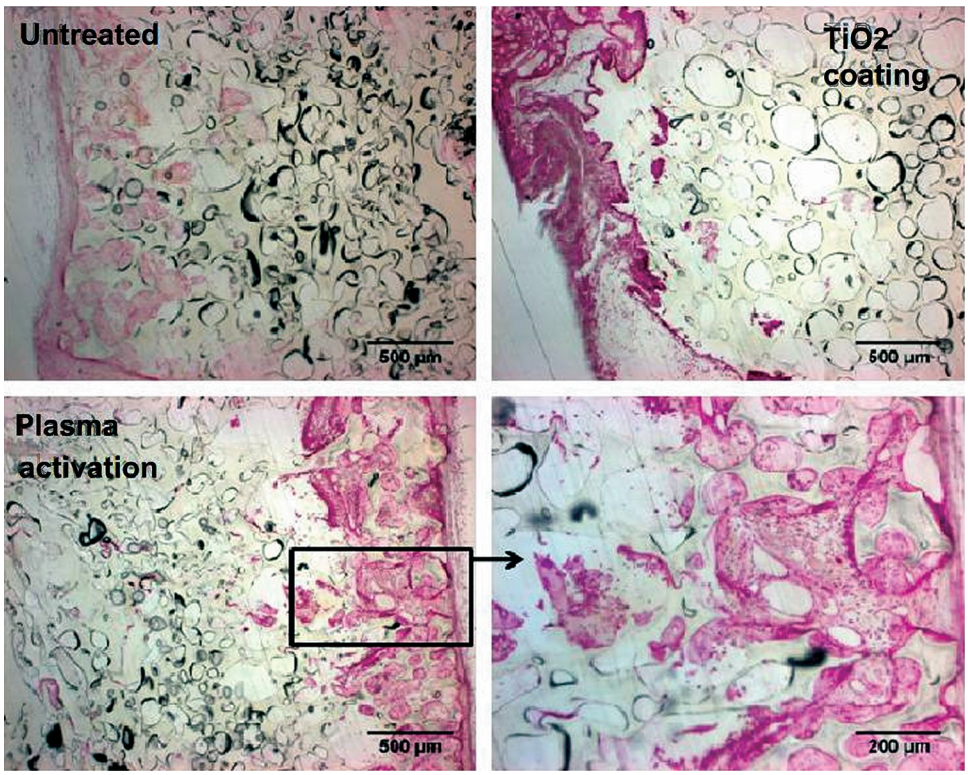

Fig. 12 Histological micrographs of implants after 24 weeks embedding time. Untreated and plasma-activated implants showed increased ingrowth of tissues and cells

Conclusion

A medical device to treat GORD has been developed where supercritical CO2 was used to produce a thermoplastic polyurethane implant with an open porous inner side to enable fixation at the implantation site. This implant was unsuccessful in a long-term pig model as the gastric implant did not show tissue ingrowth into the porous structure to prevent implant migration along the oesophagus. Additionally, the pigs suffered from dysphagia due to uncontrolled implant encapsulation. Two surface treatments, plasma and TiO2 deposition, were proposed to overcome the clinical and histological failures of the pig study. The implant surface hydrophilicity was improved after surface treatments. The in vitro tests proved that the cell attachments to the implants significantly increased after surface treatment as fibroblasts adhered to the surface and proliferated carpet-like after seven days of incubation. Both surface treatments showed higher cell ingrowth in porous structures than untreated implants. The gamma-ray sterilisation improved the cytotoxicity of implants as it led to a crosslinking of the thermoplastic polyurethane molecule chain. The vitro tests proved that the optical density decreased with the rise of gamma-ray dose, which was consistent with LIVE/DEAD® tests. Inconsistent with the in vitro finding, the TiO_2-coated implants showed the worst histocompatibility.

The cell and tissue ingrowth in the porous structure of implants were testified through in vivo studies in rabbits. Histological evidence of connective tissue was found about 1 mm deep into the gastric implants. The implants were encapsulated in fibrous tissue, as seen in the pig study, as opposed to the first in vivo study; this capsule thickness decreased with implantation time. This study shows that plasma treatment gastric implant enhanced both chemical, in vitro and in vivo response to the implant. A second pig study is planned to verify the rabbit study results and prove plasma treatment TPU indeed induce fixation around the oesophagus.

Acknowledgements The authors acknowledge the financial support of Bayerische Forschungsstiftung with Grant Number AZ639/05 and BIOMATDB funded by Horizon 2020, Grant Number 101058779.

Funding Open access funding provided by University of Oslo (incl Oslo University Hospital).

Data Availability The datasets generated during and/or analysed during the current study are available from the corresponding author on reasonable request.

Declarations

Conflict of interest The authors declare no competing interests as the original patent for this invention, EP1782760A1, by Fuessner and Haugen, has been withdrawn.

References

1. G. Boeckxstaens, H.B. El-Serag, A.J. Smout, P.J. Kahrilas, Symptomatic reflux disease: the present, the past and the future. Gut **63**(7), 1185–1193 (2014)
2. N. Mallah, J.M. Turner, F.J. Gonzalez-Barcala, B. Takkouche, Gastroesophageal reflux disease and asthma exacerbation: A systematic review and meta-analysis. Pediatr. Allergy. Immunol. **33**(1), e13655 (2022)
3. J.S. Nirwan, S.S. Hasan, Z.U. Babar, B.R. Conway, M.U. Ghori, Global prevalence and risk factors of gastro-oesophageal reflux disease (GORD): systematic review with meta-analysis. Sci. Rep. **10**(1), 5814 (2020)
4. S.K. Garg, K.S. Gurusamy, Laparoscopic fundoplication surgery versus medical management for gastro-oesophageal reflux disease (GORD) in adults. Cochrane. Database. Syst Rev (2015). https://doi.org/10.1002/14651858.CD003243.pub3
5. B.T. Johnston, The significance of heartburn. QJM **93**(6), 321–322 (2000)
6. C.P. Gyawali, D.A. Carlson, J.W. Chen, A. Patel, R.J. Wong, R.H. Yadlapati, ACG clinical guidelines: clinical use of esophageal physiologic testing. Am. J. Gastroenterol **115**(9), 1412–1428 (2020)
7. I. Hirano, J.E. Richter, Practice parameters committee of the American College of ACG practice guidelines esophageal reflux testing. Am. J. Gastroenterol **102**(3), 668–685 (2007)
8. P.O. Katz, K.B. Dunbar, F.H. Schnoll-Sussman, K.B. Greer, R. Yadlapati, S.J. Spechler, ACG clinical guideline for the diagnosis and management of gastroesophageal reflux disease. Am. J. Gastroenterol. **117**(1), 27–56 (2022)
9. R. Naguib, A.S. Alfawaz, A.M. Alqahtani, K.M. Balkhasl, R.A. Alnafee, S.N. Naji, Awareness, experience, and practice of physicians regarding adult gastroesophageal reflux disease (GERD) in Riyadh, Saudi Arabia. J. Family. Med. Prim. Care. **9**(8), 4181–4189 (2020)
10. K.M. Fock, N.J. Talley, R. Fass, K.L. Goh, P. Katelaris, R. Hunt, M. Hongo, T.L. Ang, G. Holtmann, S. Nandurkar, S.R. Lin, B.C. Wong, F.K. Chan, A.A. Rani, Y.T. Bak, J. Sollano, K.Y. Ho, S. Manatsathit, Asia-Pacific consensus on the management of gastroesophageal reflux disease: update. J. Gastroenterol. Hepatol. **23**(1), 8–22 (2008)
11. I. Schiefke, A. Zabel-Langhennig, S. Neumann, J. Feisthammel, J. Moessner, K. Caca, Long term failure of endoscopic gastroplication (EndoCinch). Gut **54**(6), 752–758 (2005)
12. M.G. Patti, An evidence-based approach to the treatment of gastroesophageal reflux disease. JAMA Surg **151**(1), 73–78 (2016)
13. M.B. Fennerty, K.B. Finke, P.R. Kushner, D.A. Peura, L. Record, L. Riley, G.E. Ruoff, W. Simonson, W.L. Wright, Short- and long-term management of heartburn and other acid-related disorders: development of an algorithm for primary care providers. J. Family. Practice **58**, 1–12 (2009)

14. B. Weber, J.E. Portnoy, A. Castellanos, M.J. Hawkshaw, D. Lurie, P.O. Katz, R.T. Sataloff, Efficacy of anti-reflux surgery on refractory laryngopharyngeal reflux disease in professional voice users: a pilot study. J. Voice. **28**(4), 492–500 (2014)
15. P. Visaggi, L. Mariani, F.B. Svizzero, L. Tarducci, A. Sostilio, M. Frazzoni, S. Tolone, R. Penagini, L. Frazzoni, L. Ceccarelli, V. Savarino, M. Bellini, P.C. Gyawali, E.V. Savarino, N. de Bortoli, Clinical use of mean nocturnal baseline impedance and post-reflux swallow-induced peristaltic wave index for the diagnosis of gastro-esophageal reflux disease. Esophagus **19**(4), 525–534 (2022)
16. S.K. McKinley, R.C. Dirks, D. Walsh, C. Hollands, L.E. Arthur, N. Rodriguez, J. Jhang, A. Abou-Setta, A. Pryor, D. Stefanidis, B.J. Slater, Surgical treatment of GERD: systematic review and meta-analysis. Surg. Endosc. **35**(8), 4095–4123 (2021)
17. M.P. Schijven, S.S. Gisbertz, M.I. van Berge Henegouwen, Laparoscopic surgery for gastro-esophageal acid reflux disease. Best Pract. Res. Clin. Gastroenterol. **28**(1), 97–109 (2014)
18. M. Bortolotti, Is patient satisfaction sufficient to validate endoscopic anti-reflux treatments? World. J. Gastroenterol. **28**(28), 3743–3746 (2022)
19. S. Ungureanu, N. Sipitco, D. Fosa, Twenty years of antireflux surgery. Retrospective of a Laparoscopic Surgery Center, Chirurgia (Bucur) 117(2) (2022) 187–197.
20. C. Mohr, H. Ciomperlik, N. Dhanani, O.A. Olavarria, C. Hannon, W. Hope, S. Roth, M.K. Liang, J.L. Holihan, Review of SAGES GERD guidelines and recommendations. Surg Endosc (2022). https://doi.org/10.1007/s00464-022-09209-7
21. A. Analatos, B.S. Hakanson, C. Ansorge, M. Lindblad, L. Lundell, A. Thorell, Clinical outcomes of a laparoscopic total vs a 270 degrees posterior partial fundoplication in chronic gastroesophageal reflux disease: a randomized clinical trial. JAMA Surg. **157**(6), 473–480 (2022)
22. J.P. Angelchik, R. Cohen, A new surgical procedure for the treatment of gastroesophageal reflux and hiatal hernia. Surg. Gynecol. Obstet. **148**(2), 246–248 (1979)
23. H. Chase, S. Mastoridis, N. Maynard, (2021) AngelChik Device Removal and Revisional Fundoplication. Journal of the Nuffield Department of Surgical Sciences. Doi: https://doi.org/10.37707/jnds.v2i2.118
24. M.W. Gear, E.W. Gillison, B.L. Dowling, Randomized prospective trial of the Angelchik anti-reflux prosthesis. Br. J. Surg. **71**(9), 681–683 (1984)
25. C. Thibault, P. Marceau, S. Biron, R.A. Bourque, L. Beland, M. Potvin, The Angelchik antireflux prosthesis: long-term clinical and technical follow-up. Can. J. Surg. **37**(1), 12–17 (1994)
26. C. Squires, R.J. Porter, B.M. Ward, Lessons from recent medical history: an obsolete anti-reflux device in an older patient with variable gastrointestinal symptoms. Age. Ageing. **50**(4), 1426–1427 (2021)
27. S. Ayazi, P. Zheng, A.H. Zaidi, K. Chovanec, M. Salvitti, K. Newhams, T. Hoppo, B.A. Jobe, Clinical outcomes and predictors of favorable result after laparoscopic magnetic sphincter augmentation: single -institution experience with more than 500 patients ? check for updates. J. Am. Coll. Surg. **230**(5), 733–743 (2020)
28. S. Joglekar, S.V. George, M. Leong, The historical Angelchik anti-reflux device: laparoscopic removal for dysphagia. ANZ. J. Surg. (2022). https://doi.org/10.1111/ans.17857
29. J. Dent, H.B. El-Serag, M.A. Wallander, S. Johansson, Epidemiology of gastro-oesophageal reflux disease: a systematic review. Gut **54**(5), 710–717 (2005)
30. H.B. Wu, E. Wintermantel, H.J. Haugen, The effects of mold design on the pore morphology of polymers produced with mucell (r) technology. J. Cell. Plast. **46**(6), 519–530 (2010)
31. H. Haugen, J. Aigner, M. Brunner, E. Wintermantel, A novel processing method for injection-molded polyether-urethane scaffolds. Part 2: Cellular interactions. J. Biomed. Mater. Res. **77B**(1), 73–78 (2006)
32. H. Haugen, L.C. Gerhardt, J. Will, E. Wintermantel, Biostability of polyether-urethane scaffolds: A comparison of two novel processing methods and the effect of higher gamma-irradiation dose. J. Biomed. Mater. Res. B. Appl. Biomater. **73B**(2), 229–237 (2005)
33. H.J. Haugen, PhD thesis: Development of an implant to treat gastro-oesophageal reflux disease, Lehrstuhl für Medizintechnik, Technical University of Munich, 2004.
34. H.J. Haugen, M. Brunner, F. Pellikofer, J. Aigner, J. Will, E. Wintermantel, Effect of different gamma-irradiation doses on cytotoxicity and material properties of porous polyether-urethane polymer. J. Biomed. Mater. Res. B. Appl. Biomater. **80B**(2), 415–423 (2007)
35. S. Leicher, J. Will, H. Haugen, E. Wintermantel, MuCell (R) technology for injection molding: A processing method for polyether-urethane scaffolds. J. Mater. Sci. **40**(17), 4613–4618 (2005)
36. H.B. Wu, E. Krampe, H. Schlicht, E. Wintermantel, Application of a microcellular injection molding process (MuCell (R)) to produce an implant with porous structure. World Congress. Med. Phys. Biomed. Eng. **25**(10), 61–64 (2009)
37. D.F. Xu, K.J. Yu, K. Qian, C.B. Park, Foaming behavior of microcellular poly(lactic acid)/TPU composites in supercritical CO2. J. Thermoplast. Compos. Mater. **31**(1), 61–78 (2018)
38. H.Y. Mi, X. Jing, M.R. Salick, X.F. Peng, L.S. Turng, A novel thermoplastic polyurethane scaffold fabrication method based on injection foaming with water and supercritical carbon dioxide as coblowing agents. Polym. Eng. Sci. **54**(12), 2947–2957 (2014)
39. X.L. Jiang, L. Zhao, L.F. Feng, C.P. Chen, Microcellular thermoplastic polyurethanes and their flexible properties prepared by mold foaming process with supercritical CO2. J. Cell. Plast. **55**(6), 615–631 (2019)
40. J. Chen, J.G. Ye, X. Liao, S.J. Li, W. Xiao, Q. Yang, G.X. Li, Organic solvent free preparation of porous scaffolds based on the phase morphology control using supercritical CO2. J. Supercrit. Fluid. **149**, 88–96 (2019)
41. J. Wang, J. Li, H. Li, H. Zhou, Thermoplastic polyurethane (TPU) modifier to develop bimodal cell structure in polypropylene/TPU microcellular foam in presence of supercritical CO2. J. Vinyl Add. Tech. **27**(1), 127–136 (2021)
42. D. Wilhelm, A. Meining, A. Schneider, S. von Delius, A. Preissel, J. Sager, A. Fiolka, H. Friess, H. Feussner, NOTES for the cardia: antireflux therapy via transluminal access. Endoscopy **42**(12), 1085–1091 (2010)
43. H. Schlicht, H. Haugen, R. Sabetrasekh, E. Wintermantel, Fibroblastic response and surface characterization of O2 plasma treated thermoplastic polyetherurethane. Biomed. Mater. **5**(025002), 1–10 (2010)
44. J. Aigner, P. Hutzler, J. Bujia, E. Kastenbauer, Distribution and viability of cultured human chondrocytes in a three-dimensional matrix as assessed by confocal laser scan microscopy. In Vitro. Cell. Dev-An. **33**(6), 407–409 (1997)
45. B. Gabryel, M. Adamek, A. Pudelko, A. Malecki, H.I. Trzeciak, Piracetam and vinpocetine exert cytoprotective activity and prevent apoptosis of astrocytes in vitro in hypoxia and reoxygenation. Neurotoxicology **23**(1), 19–31 (2002)
46. S. Rammelt, D. Corbeil, S. Manthey, H. Zwipp, U. Hanisch, Immunohistochemical in situ characterization of orthopedic implants on polymethyl metacrylate embedded cutting and grinding sections. J. Biomed. Mater. Res., Part A **83**(2), 313–322 (2007)
47. H.Y. Mi, X. Jing, M.R. Salick, T.M. Cordie, X.F. Peng, L.S. Turng, Properties and fibroblast cellular response of soft and hard

thermoplastic polyurethane electrospun nanofibrous scaffolds. J. Biomed. Mater. Res. **103**(5), 960–970 (2015)
48. A. Lis-Bartos, A. Smieszek, K. Franczyk, K. Marycz, Fabrication, characterization, and cytotoxicity of thermoplastic polyurethane/poly(lactic acid) material using human adipose derived mesenchymal stromal stem cells (hASCs). Polymers (Basel) **10**(10), 1073 (2018)
49. S. Sharifpoor, R.S. Labow, J.P. Santerre, Synthesis and characterization of degradable polar hydrophobic ionic polyurethane scaffolds for vascular tissue engineering applications. Biomacromol **10**(10), 2729–2739 (2009)
50. J.E. McBane, D. Ebadi, S. Sharifpoor, R.S. Labow, J.P. Santerre, Differentiation of monocytes on a degradable, polar, hydrophobic, ionic polyurethane: Two-dimensional films vs three-dimensional scaffolds. Acta. Biomater. **7**(1), 115–122 (2011)
51. P. Alves, S. Pinto, H.C. de Sousa, M.H. Gil, Surface modification of a thermoplastic polyurethane by low-pressure plasma treatment to improve hydrophilicity. J. Appl. Polym. Sci. **122**(4), 2302–2308 (2011)
52. M. Rahmati, E.A. Silva, J.E. Reseland, A.H. C, H.J. Haugen, Biological responses to physicochemical properties of biomaterial surface. Chem. Soc. Rev. **49**(15), 5178–5224 (2020)
53. J.A. Pan, H.L. Liu, W.T. Ting, H.K. Hsu, K.S. Chen, Surface modification by deposition of IPA plasma and gellan gum/chitosan hybrid hydrogel onto thermoplastic polyurethane for controlled release of N-acetylcysteine. J. Chin. Chem. Soc. **66**(7), 691–697 (2019)
54. Z.W. Ma, G. Changyou, Y. Jun, Ji. Jian, G. Yihong, S. Jiacong, Surface modification of poly-L-lactide by photografting of hydrophilic polymers towards improving its hydrophilicity. J. Appl. Polym. Sci. **85**(10), 2163–2171 (2002)
55. P.K. Chu, J.Y. Chen, L.P. Wang, N. Huang, Plasma-surface modification of biomaterials. Mater. Sci. Eng. **36**, 143–206 (2002)
56. H.R. Lim, H.S. Baek, M.H. Lee, Y.I. Woo, D.-W. Han, M.H. Han, H.K. Baik, W.S. Choi, Surface modification for enhancing behaviors of vascular endothelial cells onto polyurethane films by microwave-induced argon plasma. Surf. Coat. Technol. **202**, 5768–5772 (2008)
57. D. Gantz, S. Bertoldi, N. Contessi Negrini, H.J. Haugen, Polymers and scaffolds with improved blood compatibility and enhanced cellular response with focus on polyurethane foams functionalized with amino-amide groups. J. Adv. Biotechnol. Bioeng. **7**, 18–29 (2019)
58. G.A. Venegas-Cervera, A.I. Oliva, A. Avila-Ortega, J.M. Cervantes-Uc, L.M. Carrillo-Cocom, J.A. Juarez-Moreno, Biocompatibility studies of polyurethane electrospun membranes based on arginine as chain extender. J. Mater. Sci. Mater. Med. **32**(9), 104 (2021)
59. Y.L. Uscategui, L.E. Diaz, M.F. Valero, In vitro and in vivo biocompatibility of polyurethanes synthesized with castor oil polyols for biomedical devices. J. Mater. Res. **34**(4), 519–531 (2019)
60. A.C. Stromdahl, L. Ignatowicz, G. Petruk, M. Butrym, S. Wasserstrom, A. Schmidtchen, M. Puthia, Peptide-coated polyurethane material reduces wound infection and inflammation. Acta. Biomater. **128**, 314–331 (2021)
61. X. Cheng, J. Fei, A. Kondyurin, K. Fu, L. Ye, M.M.M. Bilek, S. Bao, Enhanced biocompatibility of polyurethane-type shape memory polymers modified by plasma immersion ion implantation treatment and collagen coating: An in vivo study. Mater. Sci. Eng. C **99**, 863–874 (2019)
62. M.R. Sanchis, O. Calve, O. Fenollar, D. Garcia, R. Balart, Surface modification of a polyurethane film by low pressure glow discharge oxygen plasma treatment. J. Appl. Polym. Sci. **105**(3), 1077–1085 (2007)
63. L. Wang, Y. Li, Y. Zuo, L. Zhang, Q. Zou, L. Cheng, H. Jiang, Porous bioactive scaffold of aliphatic polyurethane and hydroxyapatite for tissue regeneration. Biomed. Mater. **4**(2), 025003 (2009)
64. P. Buma, N.N. Ramrattan, T.G. van Tienen, R.P.H. Veth, Tissue engineering of the meniscus. Biomaterials **25**(9), 1523–1532 (2004)
65. A.J. Schouten, R.G.J.C. Heijkants, R.V. Van Calck, J.H. De Groot, A.J. Pennings, T.G. Van Tienen, N. Ramrattan, P. Buma, R.P.H. Veth, Design, synthesis and properties of a degradable polyurethane scaffold for meniscus regeneration. J. Mater. Sci. Mater. Med. **15**(4), 423–427 (2004)
66. L. De Nardo, S. Bertoldi, M.C. Tanzi, H.J. Haugen, S. Fare, Shape memory polymer cellular solid design for medical applications. Smart. Mater. Struct. (2011). https://doi.org/10.1088/0964-1726/20/3/035004
67. A. Uricchio, E. Nadal, B. Plujat, G. Plantard, F. Massines, F. Fanelli, Low-temperature atmospheric pressure plasma deposition of TiO2-based nanocomposite coatings on open-cell polymer foams for photocatalytic water treatment. Appl. Surf. Sci. **561**, 150014 (2021)
68. P. Hajkova, Plasma treatment & surface modification, Int C Chem Technol (2019) 122–126.
69. V. Armenise, F. Fanelli, A. Milella, L. D'Accolti, A. Uricchio, F. Fracassi, Atmospheric pressure plasma treatment of polyurethane foams with He-O-2 fed dielectric barrier discharges. Surf. Interfaces. (2020). https://doi.org/10.1016/j.surfin.2020.100600
70. Z. Niu, X. Jia, W. Zhang, W. Chen, K. Qian, Reactive spuutering TiO_2 films for surface coating of poly(dimethylsiloxane). Appl. Surf. Sci. **252**, 2259–2264 (2006)
71. A. Jorda-Vilaplana, L. Sanchez-Nacher, D. Garcia-Sanoguera, A. Carbonell, J.M. Ferri, Effects of aging on the adhesive properties of poly(lactic acid) by atmospheric air plasma treatment. J. Appl. Polym. Sci. (2016). https://doi.org/10.1002/app.43040
72. A. Jorda-Vilaplana, V. Fombuena, D. Garcia-Garcia, M.D. Samper, L. Sanchez-Nacher, Surface modification of polylactic acid (PLA) by air atmospheric plasma treatment. Eur. Polym. J. **58**, 23–33 (2014)
73. S. Takemoto, T. Yamamoto, K. Tsuru, S. Hayakawa, A. Osaka, S. Takashima, Platelet adhesion on titanium oxide gels: effect of surface oxidation. Biomaterials **25**(17), 3485–3492 (2004)
74. Y. Arima, H. Iwata, Effect of wettability and surface functional groups on protein adsorption and cell adhesion using well-defined mixed self-assembled monolayers. Biomaterials **28**(20), 3074–3082 (2007)
75. J. Matinha-Cardoso, R. Mota, L.C. Gomes, M. Gomes, F.J. Mergulhao, P. Tamagnini, M.C.L. Martins, F. Costa, Surface activation of medical grade polyurethane for the covalent immobilization of an anti-adhesive biopolymeric coating. J. Mater. Chem. B **9**(17), 3705–3715 (2021)
76. B.S. Cho, S.T. Noh, Thermal properties of polyurethane binder with 2-(ferrocenylpropyl)dimethylsilane-grafted hydroxyl-terminated polybutadiene. J. Appl. Polym. Sci. **121**(6), 3560–3568 (2011)
77. N. Xiang, X.W. Zhang, M.Y. Zheng, Y. Ge, T. Wang, H.B. Liu, C. Maharaj, J.P. Dear, Y. Yan, Microstructure and tensile properties of injection molded thermoplastic polyurethane with different melt temperatures. J. Appl. Polym. Sci. **137**(29), 48891 (2020)
78. E. Adem, E. Angulo-Cervera, A. Gonzalez-Jimenez, J.L. Valentin, A. Marcos-Fernandez, Effect of dose and temperature on the physical properties of an aliphatic thermoplastic polyurethane irradiated with an electron beam. Radiat. Phys Chem. **112**, 61–70 (2015)
79. A. Ashfaq, M.C. Clochard, X. Coqueret, C. Dispenza, M.S. Driscoll, P. Ulanski, M. Al-Sheikhly, Polymerization reactions and modifications of polymers by ionizing radiation. Polymers (Basel) **12**(12), 2877 (2020)

80. H. Munstedt, Mechanical pretreatment of polymer melts: Critical aspects and new rheological investigations on a linear and a long-chain branched polypropylene. J. Rheol. **65**(5), 871–885 (2021)
81. F. Koper, T. Swiergosz, A. Zaba, A. Flis, M. Travnickova, L. Bacakova, E. Pamula, D. Bogdal, W.P. Kasprzyk, Advancements in structure-property correlation studies of cross-linked citric acid-based elastomers from the perspective of medical application. J. Mater. Chem. B **9**(32), 6425–6440 (2021)
82. A.S. Gubarev, A.A. Lezov, N.G. Mikusheva, I. Perevyazko, A.S. Senchukova, A.A. Lezova, A.N. Podsevalnikova, V.B. Rogozhin, M. Enke, A. Winter, U.S. Schubert, N.V. Tsvetkov, Hydrodynamic characteristics and conformational parameters of ferrocene-terpyridine-based polymers. Polymers (Basel) **14**(9), 1776 (2022)
83. K. Krol-Morkisz, E. Karas, T.M. Majka, K. Pielichowski, K. Pielichowska, Thermal stabilization of polyoxymethylene by PEG-functionalized hydroxyapatite: examining the effects of reduced formaldehyde release and enhanced bioactivity. Adv Polym Tech (2019). https://doi.org/10.1155/2019/9728637
84. K. Espinoza-Garcia, A. Marcos-Fernandez, R. Navarro, A. Ramirez-Hernandez, J.E. Baez-Garcia, G. Rangel-Porras, Polymerization of epsilon-caprolactone with degraded PET for its functionalization. J. Polym. Res. (2019). https://doi.org/10.1007/s10965-019-1821-6
85. C. Botha, J.F. Kuntz, C. Moire, C. Farcet, H. Pfukwa, H. Pasch, Molar mass analysis of hydrophobically modified hyaluronic acid by SEC-MALLS: facing the challenges of amphiphilic biomacromolecules. Macromol. Chem. Phys. (2018). https://doi.org/10.1002/macp.201800233
86. Q. Carboue, S. Fadlallah, M. Lopez, F. Allais, Progress in degradation behavior of most common types of functionalized polymers: a review. Macromol. Rapid. Commun. **43**(13), e2200254 (2022)
87. R. Andler, T. Tiso, L. Blank, C. Andreessen, J. Zampolli, V. D'Afonseca, C. Guajardo, A. Diaz-Barrera, Current progress on the biodegradation of synthetic plastics: from fundamentals to biotechnological applications. Rev. Environ. Sci. Bio. **21**, 829–850 (2022)
88. H.Y. Mi, M.R. Salick, X. Jing, B.R. Jacques, W.C. Crone, X.F. Peng, L.S. Turng, Characterization of thermoplastic polyurethane/polylactic acid (TPU/PLA) tissue engineering scaffolds fabricated by microcellular injection molding. Mater. Sci. Eng. **33**(8), 4767–4776 (2013)
89. H.Y. Mi, X. Jing, M.R. Salick, L.S. Turng, X.F. Peng, Fabrication of thermoplastic polyurethane tissue engineering scaffold by combining microcellular injection molding and particle leaching. J. Mater. Res. **29**(8), 911–922 (2014)
90. K. Kawaguchi, Y. Tajima, Crystalline morphology of injection-molded polyacetal with branched structure. Kobunshi Ronbunshu **62**(3), 124–130 (2005)
91. N.Y. Ning, F. Luo, K. Wang, Q. Zhang, F. Chen, R.N. Du, C.Y. An, B.F. Pan, Q. Fu, Molecular weight dependence of hybrid shish kebab structure in injection molded bar of polyethylene/inorganic whisker composites. J. Phys. Chem. B **112**(45), 14140–14148 (2008)
92. M. Wang, L. Xu, M. Zhai, J. Peng, J. Li, G. Wei, g-ray radiation-induced synthesis and Fe(III) ion adsorption of carbosymethylated chitosan hydrogels. Carbohyd. Polym. **74**, 498–503 (2008)
93. Y. Zhang, S. Zhao, Y. Li, L. Xie, K. Sheng, Radiation effects on styrene-butadiene-styrene copolymer. Nucl. Inst. Methods Phys. Res. B **266**, 3431–3436 (2008)
94. G. Djafar, B. Abbas, Radiation crosslinking of LDPE and HDPE with 5 and 10 MeV electron beams. Eur. Polym. J. **37**(10), 2011–2016 (2001)
95. A. Simmons, J. Hyvarinen, L. Poole-Warren, The effect of sterilisation on a poly(dimethylsiloxane)/poly(hexamethylene oxide) mixed macrodiol-based polyurethane elastomer. Biomaterials **27**, 4484–4497 (2006)
96. C. Zahraoui, P. Sharrock, Influence of sterilization on injectable bone biomaterials. Bone **25**(1), 63S-65S (1999)
97. K. Gorna, S. Gogolewski, The effect of gamma radiation on molecular stability and mechanical properties of biodegradable polyurethanes for medical applications. Polym. Degrad. Stabil. **79**, 465–474 (2003)
98. C. Guignot, N. Betz, B. Legendre, A. Le Moel, N. Yagoubi, Degradation of segmented poly(etherurethane) Tecoflex induced by electron beam irradiation: Characterization and evaluation. Nucl. Inst. Methods Phys. Res. B **185**, 100–107 (2001)
99. J. Wei, O.Z. Chen, M.M. Stevens, J.A. Roether, A.R. Boccaccini, Biocompatibility and bioactivity of PDLLA/TiO_2 and PDLLA/TiO_2/Bioglass® nanocomposites. Mater. Sci. Eng. C **28**, 1–10 (2008)
100. Z.H. Dong, Y.B. Li, Q. Zou, Degradation and biocompatibility of porous nano-hydroxyapatite/polyurethane composite scaffold for bone tissue engineering. Appl. Surf. Sci. **255**(12), 6087–6091 (2009)
101. R.S. Labow, E. Meek, J.P. Santerre, Hydrolytic degradation of poly(carbonate)-urethanes by monocyte-derived macrophages. Biomaterials **22**, 3025–3033 (2001)
102. L. Bacakova, E. Filova, M. Parizek, T. Ruml, V. Svorcik, Modulation of cell adhesion, proliferation and differentiation on materials designed for body implants. Biotechnol. Adv. **29**(6), 739–767 (2011)
103. H. Rauscher, O. Kylian, J. Benedikt, A. von Keudell, F. Rossi, Elimination of biological contaminations from surfaces by plasma discharges: chemical sputtering. ChemPhysChem **11**(7), 1382–1389 (2010)
104. Y.C. Hong, H.J. Park, B.J. Lee, W.S. Kang, H.S. Uhm, Plasma formation using a capillary discharge in water and its application to the sterilization of E. coli. Phys. Plasmas. **17**(5), 053502 (2010)
105. P. Messerer, H. Halfmann, M. Czichy, M. Schulze, P. Awakowicz, Plasma sterilisation and surface modification of thermolabile materials, Surface Engineering in Materials Science Iii (2005) 205–214.
106. S.A. Hacking, J.D. Bobyn, K.-K. Toh, M. Tanzer, J.J. Krygier, Fibrous tissue ingrowth and attachment to porous tantalum. J. Biomed. Mater. Res. **52**(4), 631–638 (2000)
107. J. Schlotthauer, Polymer Characterization for Soft-Tissue Fixation Devices, Mechanical Engineering Department, University of Wyoming, Accessed Nov 2022: https://mountainscholar.org/handle/20.500.11919/2242, 2022.
108. C.A. Homsy, Soft porous PTFE-composite alloplasts: tissue-bonding characteristics. J. Endourol. **14**(1), 25–32 (2000)
109. N. Galatenko, D. Kulyesh, A. Maletskyi, O. Karpenko, Soft-tissue response to synthetic polymer implants made of cross-linked polyurethane and containing a biologically active substance, albucid or dacarbazine, in animals. J. Ophthalmol. **77**, 52–58 (2018)
110. K. Lehle, S. Lohn, G. Reinerth, T. Schubert, J.G. Preuner, D.E. Birnbaum, Cytological evaluation of the tissue-implant reaction associated with subcutaneous implantation of polymers coated with titaniumcarboxonitride in vivo. Biomaterials **25**, 5457–5466 (2004)
111. J.Y.J. Yan, F.W. Cooke, P.S. Vaskelis, A.F. von Recum, Titaniumcoated Dacron velour: a study of interfacial connective tissue formation. J. Biomed. Mater. Res. **23**(2), 171–189 (1989)
112. C. Shannon, R. Thull, A. Von Recum, Types I und III collagen in the tissue capsules of titanium and stainless-steel implants. J. Biomed. Mater. Res. **34**, 401–408 (1997)